

UNCLASSIFIED

AD NUMBER

AD250504

LIMITATION CHANGES

TO:

Approved for public release; distribution is unlimited.

FROM:

Distribution authorized to U.S. Gov't. agencies and their contractors;
Administrative/Operational Use; OCT 1960. Other requests shall be referred to Air Force Cambridge Research Laboratory, Hanscom AFB, MA.

AUTHORITY

afcr1 ltr 3 nov 1971

THIS PAGE IS UNCLASSIFIED

UNCLASSIFIED

AD 250 504

*Reproduced
by the*

**ARMED SERVICES TECHNICAL INFORMATION AGENCY
ARLINGTON HALL STATION
ARLINGTON 12, VIRGINIA**



UNCLASSIFIED

NOTICE: When government or other drawings, specifications or other data are used for any purpose other than in connection with a definitely related government procurement operation, the U. S. Government thereby incurs no responsibility, nor any obligation whatsoever; and the fact that the Government may have formulated, furnished, or in any way supplied the said drawings, specifications, or other data is not to be regarded by implication or otherwise as in any manner licensing the holder or any other person or corporation, or conveying any rights or permission to manufacture, use or sell any patented invention that may in any way be related thereto.

VP

260504
J NO. —
ASTIA FILE COPY

**AN EXPERIMENTAL INVESTIGATION OF NEGATIVE
POINT-PLANE CORONA AND ITS RELATION TO
BALL LIGHTNING**

FINAL REPORT

Prepared by

Edward T. Pierce
Richard M. Nadile
Philip J. McKinnon

Research and Advanced Development Division
Avco Corporation
Wilmington, Massachusetts

Technical Report

RAD-TR-60-29

Contract AF19(604)-7342

24 October 1960

61-2-1
XEROX

ASTIA
RECEIVED
FEB 13 1961
TIPDR

Prepared for

AIR FORCE RESEARCH DIRECTORATE
CAMBRIDGE RESEARCH LABORATORIES
AIR FORCE RESEARCH DIVISION
AIR RESEARCH AND DEVELOPMENT COMMAND
UNITED STATES AIR FORCE
Bedford, Massachusetts

XEROX

750 650

**AN EXPERIMENTAL INVESTIGATION OF NEGATIVE
POINT-PLANE CORONA AND ITS RELATION TO
BALL LIGHTNING**

FINAL REPORT

Prepared by


Edward T. Pierce
Richard M. Nadile
Philip J. McKinnon


Research and Advanced Development Division
Avco Corporation
Wilmington, Massachusetts

Technical Report
RAD-TR-60-29
Contract AF19(604)-7342

24 October 1960

APPROVED


S. C. Coroniti
Chief, Geophysics Section


J. A. Kyger
Vice President

Prepared for

ELECTRONICS RESEARCH DIRECTORATE
AIR FORCE CAMBRIDGE RESEARCH LABORATORIES
AIR FORCE RESEARCH DIVISION
AIR RESEARCH AND DEVELOPMENT COMMAND
UNITED STATES AIR FORCE
Bedford, Massachusetts

Requests for additional copies by Agencies of the Department of Defense, their contractors, and other Government agencies should be directed to the:

ARMED SERVICES TECHNICAL INFORMATION AGENCY
ARLINGTON HALL STATION
ARLINGTON 12, VIRGINIA

Department of Defense contractors must be established for ASTIA services or have their "need-to-know" certified by the cognizant military agency of their project or contract.

All other personnel and organizations should apply to the:

U. S. DEPARTMENT OF COMMERCE
OFFICE OF TECHNICAL SERVICES
WASHINGTON 25, D. C.

ABSTRACT

Existing theories of ball lightning are briefly discussed. Kapitsa has suggested that the energy to sustain a fireball comes from resonant absorption of radio waves of 300/mc/s. Pierce has extended Kapitsa's theory* by suggesting a mechanism for producing this r-f energy during a corona discharge. The corona discharge from a negative point flows in a series of regular pulses called trichel pulses. Based on the theoretical relationship between corona discharge (Trichel pulses) and ball lightning, an experimental program is developed.

The main part of this report is concerned with the description and discussion of the experiments. To obtain the maximum possible corona frequencies, a van de Graaff generator has been utilized. An applied voltage of 280,000 volts has produced a current of 125 microamperes and a Trichel pulse frequency above 2 mc/s. This short experiment has established the usefulness of this type of generator.

The experiment, however, has been conducted with a small d-c high-voltage generator (up to 30 kv). Several types of points have been used. An attempt has also been made to stabilize the Trichel pulse frequency with an applied resonating frequency. This method has been successful on one occasion; namely, when a 10 kc/s Trichel pulse frequency has been stabilized with a 10 kc/s sine wave. Monitoring of the Trichel pulses is usually performed electronically, but a technique has been developed to monitor them photoelectrically for purposes of comparison.

Pulse-repetition frequencies of a few mc/s have been the highest attained in the course of the experiments. The results obtained are then discussed as they concern ball lightning.

*Pierce, E. T., Avco Proposal (1959).

ACKNOWLEDGMENTS

We are grateful to Dr. B. Washburn, Director of the Museum of Science, Boston, Massachusetts and to Mr. J. Hughes, Office of Naval Research for making the van de Graaff generator available to us. We are particularly indebted to Mr. Glen Armstrong of the Museum of Science, and Lieutenant Commander Ronald Winder, USNR, for operating the van de Graaff machine, and assisting us in conducting the experiments.

We wish to thank Mr. R. Pagliarulo for his extensive assistance in some of the measurements, in the data reduction, and in the editing of the report.

The assistance of Mr. S. Forman and Mr. G. Gagne in the preparation of the experiments at the Museum of Science, and Miss D. Salmas in the data reduction is gratefully acknowledged.

We wish to express our appreciation to Mr. S.C. Coroniti for his suggestions and the very helpful discussions of the problem.

CONTENTS

I. Introduction	1
1.1 Ball Lightning	1
1.2 Point Corona in Air at Normal Temperatures and Pressures	2
1.3 Negative Point Corona -- Fine Structure	4
1.4 Natural Point Discharge	9
1.5 Experimental Work	20
II. Experimental Work at Boston Museum of Science	28
III. Trichel Pulse Corona	28
3.1 General Features of the Pulsed Corona	28
3.2 Simultaneously Occurring Families of Pulses	33
3.3 Standard Deviation of Pulse Intervals	40
3.4 Stabilization of Trichel Pulse Discharge	44
3.5 Current-Frequency Relationships	54
3.6 Photoelectric and Audio Technique	62
IV. Discussion, Conclusions, and Suggestions for Further Work	68
V. References	70

ILLUSTRATIONS

Figure	1	Mechanism of Trichel Pulse Corona	5
	2	Mechanism of Trichel Pulse Corona	6
	3	Constant Characteristic of Gap A_s versus Angular Frequency s	10
	4	Spectrum of Single Pulse S_p versus Angular Frequency s	11
	5	Amplitude Distribution $G(s)$ versus Angular Frequency s for $\tau = 10^{-6}$ sec	12
	6	Amplitude Distribution $G(s)$ versus Angular Frequency s for $\tau = 10^{-7}$ sec	13
	7	Sequence of Events in Flash to Earth	17
	8	S_p Plotted against Frequency f for $\tau = 10^{-8}$ sec	21
	9	Corona Current versus Applied Voltage	24
	10	Corona Current versus Pulse Repetition Frequency	25
	11	Applied Voltage versus Pulse Repetition Frequency	26
	12	Schematic Diagram of Equipment	29
	13	Corona Current versus Applied Voltage for Different Point-Plane Separations	30
	14	Multi-Family Trichel Pulses	34
	15	Small and Medium Trichel Pulses	35
	16	Small Trichel Pulses	36
	17	Characteristics of Multi-Family Trichel Pulses	38
	18	Family Pulses Considered Separately	39
	19	Frequency Spectrum (85 kc/s - 350 c/s)	41

ILLUSTRATIONS (Cont'd)

Figure 20	Ten kc/s Pulses	42
21	Panoramic Analyzer Display (10 kc/s).....	43
22	Histogram of Pulse Intervals (10 kc/s).....	45
23	Twenty kc/s Pulses.....	46
24	Panoramic Analyzer Display (20 kc/s).....	47
25	Histogram of Pulse Intervals (20 kc/s).....	48
26	Trichel Pulses (10 kc/s)	50
27	Synchronization of 10 kc/s Trichel Pulses with 10 kc/s Sine Wave	51
28	Enlarged Section of Figure 26	52
29	Enlarged Section of Figure 27	53
30	Histogram of 10 kc/s Unsynchronized Pulse Intervals	55
31	Histogram of 10 kc/s Synchronized Pulse Intervals	56
32	Schematic Diagram of Equipment	57
33	Unsynchronized Trichel Pulses	58
34	Corona Current versus Trichel Pulse Repetition Frequency	59
35	Applied Voltage versus Trichel Pulse Repetition Frequency	60
36	Corona Current versus Trichel Pulse Repetition Frequency	61
37	Schematic Diagram of Photoelectric Technique	63
38	Ten kc/s Photoelectric Pulses	64

ILLUSTRATIONS (Cont'd)

Figure 39	Twenty kc/s Photoelectric Pulses	65
40	Ten kc/s Photoelectric and Electric Pulses	66
41	Twenty kc/s Photoelectric and Electric Pulses	67

I. INTRODUCTION

1.1 Ball Lightning

The very existence of ball lightning has aroused considerable scientific skepticism over many years. An important factor in determining this attitude is the lack of reports on this phenomenon by professional observers such as meteorologists. In consequence, the whole subject has acquired an aura of doubt.

Nevertheless, there are recent indications of a change of climate and an awakening of interest. Most geophysicists are no longer prepared to dismiss ball lightning as merely hallucinatory, and consider that the consistency of many of the reported observations implies that the phenomenon even if not understood is definitely a reality. This altered attitude is illustrated by two quotations from the works of Schonland, perhaps the foremost world authority on lightning. Schonland, writing in 1950,¹ speaks of theories of ball lightning being "not at present of much interest...in the absence of reliable observations." By 1956 his attitude has become somewhat less severe. Schonland, in a survey of lightning,² after giving a brief description of ball lightning, closes with the objective statement, "Well authenticated cases of this phenomenon are rare and it will not be discussed here."

It is not the purpose of this investigation to give detailed information on the phenomenology of ball lightning; however, to clarify some of the arguments that follow, a brief working description is desirable. In accordance with the most usual accounts, ball lightning will be taken to imply a luminous sphere appearing on or near the ground immediately following a discharge to earth. The sphere may persist for several seconds; it is on the average perhaps a foot (30 cm) in diameter, and can vanish either explosively or quietly.

Theories of ball lightning are few but diversified. A quantum theory of the phenomenon exists,³ and there are also explanations involving the combustion of atmospheric vapors. Nauer, following a detailed study,⁴ favors the latter approach, and he is supported in this view by Hill,^{5, 6} who considers that in addition to vapor combustion, other influences are important, notably hydrodynamic vortices and the heating of dust particles. However, most theories of ball lightning are founded upon the premise that some kind of protracted electrical discharge is involved. Several Russian authors^{7, 8, 9} have recently published work along these lines, and it is one of these papers, (Kapitsa⁹) that has supplied the original stimulus for the work described in this report.

In his paper, Kapitsa points out that the energy stored internally in the fire-ball at its outset is quite insufficient to maintain the ball in existence for times of the order of a second. Consequently, there must be an external

source supplying the energy. Kapitsa suggests that the required source lies in radio-frequency waves, whose generation is associated with the presence of the thunderstorm, and which are resonantly absorbed within the ball when the wavelength of the incident radio energy is 3.65 times the diameter of the ball; under these circumstances the system is in equilibrium, with a frequency of the incoming radio waves of about 300 mc/s (wavelength $3.65 \times 30 = 109.5$ cm).

There are two obvious difficulties in the Kapitsa theory. Firstly, the source of the radio-frequency energy is obscure, and if it is within the thundercloud, as implied by Kapitsa, is far-removed from the surface of the earth, the most common location for the fireball. Secondly, and more importantly, the presence of any resonance effects for specific dimensions of the fireball implies that the radio waves must be concentrated at discrete frequencies, and Kapitsa gives no indication of how this can occur.

The first author of this report has suggested¹⁰ a mechanism whereby the difficulties can to some extent be avoided. A discharge to earth almost always brings down negative electricity to the ground.^{11, 12, 13} Before the flash the potential gradient is negative, and consequently point-discharge (also known as corona or in its extreme form as St. Elmo's Fire) from sharp objects upon the surface of the ground produces a positive space charge in the lower atmosphere. Immediately after the discharge the field is reversed and the point-discharge from the ground is a corona from negative points. As such, it is intrinsically pulsed¹⁴ (being of the Trichel pulse type¹⁵), and the radiated radio energy is concentrated at the pulse repetition frequency and its harmonics.¹⁶ It is suggested that the radiation from points in negative corona furnishes the radio energy required by Kapitsa's theory for the maintenance of the fireball, and that this mechanism overcomes the major difficulties in the original Kapitsa paper by providing a radiator in close proximity to the phenomenon, and a radio frequency spectrum which is inherently of a line type. The implications, disadvantages, possible tests, and developments of this suggestion form the stimulus for the work in this report.

1.2 Point Corona in Air at Normal Temperatures and Pressures

Corona breakdown and currents can best be understood in relation to the two Townsend coefficients of α and $\gamma \cdot \alpha$, the primary coefficient, represents the intensification of current due to ionization by electron collision in the gas. If n_x is the number of electrons at any point x (measured along the field direction), then the increase dn in the number of electrons over a distance dx is given by,

$$dn = \alpha n_x dx \quad (1)$$

which may be integrated to yield,

$$n_x = n_0 e^{\alpha x} \quad , \quad (2)$$

where n_0 is the initial number of electrons. Thus one electron would produce an electron avalanche of $e^{\alpha x}$ electrons in traveling the distance x . n_x and n_0 can be replaced in equation (2) by i_x and i_0 as terms representing the current since there is a direct proportionality.

α only refers to the magnification of the current by the field. With highly non-uniform field configurations, as is always the case in point corona phenomena, integration is necessary to determine the current magnification. It is also essential, if the process is to continue, that the favorably placed electron which initiated the corona should be replaced by a secondary electron arising as a result of the α intensification in the gas. The corona will then be regenerative. γ , the second Townsend coefficient, may be defined by stating that,

$$\gamma dn = \gamma \alpha n_x dx \quad , \quad (3)$$

will be the number of secondary electrons produced as the result of the appearance of dn primary electrons. The combination of the α and γ processes leads, in many instances, to the well-known expression,

$$i_x = \frac{i_0 e^{\alpha x}}{1 - \gamma(e^{\alpha x} - 1)} \quad . \quad (4)$$

It can be seen from equation (4) that the current is intensified both as a result of a finite α and of a finiteness γ .

The γ coefficient may entail several mechanisms. The most important of these are the electrode processes of emission by ion (γ_i) and photon (γ_p) bombardment, and photo-ionization in the gas (especially significant at high pressures). Other agencies that have claims, under certain circumstances, to be considered as included in the γ coefficient are the action of metastable atoms in the gas or at the electrode; positive ion impact in the gas; field emission; and thermionic emission.

Most laboratory work on point-plane corona has been conducted with two geometries. The use of a configuration in which the electrodes are confocal paraboloids¹⁷ has the advantage that the electric field can easily be calculated, and this is also the case for a hyperboloidal point and a plane.¹⁸ However, the difficulties in the manufacture of such arrangements more than outweigh the advantages of their use. Accordingly, point-plane configurations are normally employed in which the point is a hemispherically capped cylinder,¹⁹ or, more commonly, merely a cone with a rounded end.

When a d-c voltage V is applied to a point-plane gap, the corona current I from the point obeys the following kind of relation,

$$I = A(V)(V - V_s) \quad (5)$$

where A is a constant characteristic of the gap, and V_s is the voltage at which the corona starts. The onset voltage V_s is primarily governed by the distribution of electric field in the immediate vicinity of the point, or in other words it is dependent upon the radius r of the point. The sharper the point the smaller the value of V_s . The constant A is indicative of the speed with which ions are removed from the vicinity of the point; it is therefore controlled by the fields across the gap and dependent both upon r and on the width d of the gap to a relative degree governed by the actual values of r and d .

1.3 Negative Point Corona--Fine Structure

It was originally noted by Marcus O'Day²⁰ that the corona discharge from a negative point usually flows in a series of regular pulses. These pulses were subsequently examined by Trichel¹⁵ and are commonly termed Trichel pulses. Several other investigations of Trichel pulses have been carried out by Loeb and his school, including the detailed work of Amin²¹ upon the fine structure.

For voltages only slightly larger than V_s the Trichel pulses are somewhat random and irregular, but as the voltage across the gap is further increased, the pulses become extremely regular and the succession resembles a relaxation oscillation. For a given geometry, each pulse carries a definite quantum m of charge and increase in current is manifest as a proportionate increase in pulse repetition frequency F . The relation is,

$$I = mF \quad (6)$$

This is obeyed over a considerable range in voltage but eventually, as current continues to increase, there are divergencies from the linear law in the sense that the frequency grows more rapidly than does the current; this implies a decrease in the quantum of charge per pulse. Both Bandel²² and Greenwood²³ have noted that a further increase in current often results in the disappearance of the Trichel pulses. The discharge is of a continuous Townsend type, presumably because negative ion formation is no longer capable of the choking effect necessary for the generation of the Trichel pulses. Further increase of voltage beyond the Townsend regime leads to breakdown of the gap.

The mechanism of Trichel pulse corona is indicated on figures 1 and 2 which follow the ideas outlined by Amin.²¹ A typical pulse is initiated by a single electron avalanche which is augmented by other avalanches due to electron

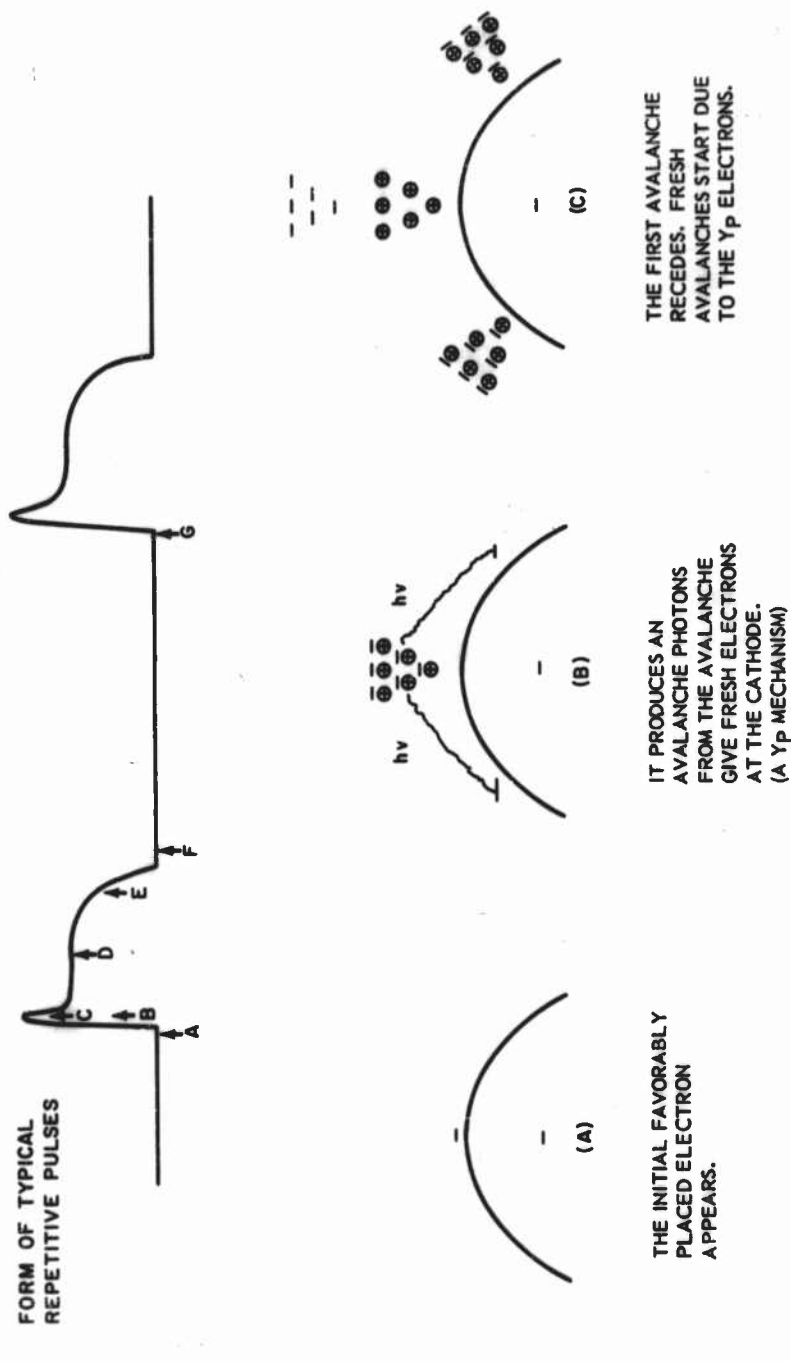
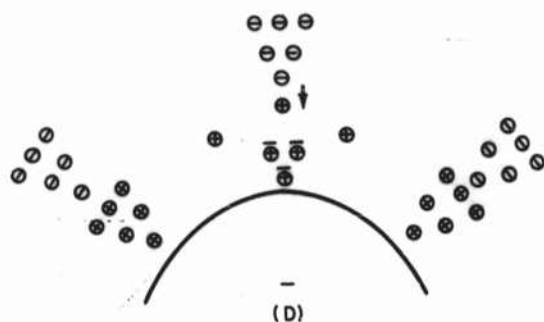
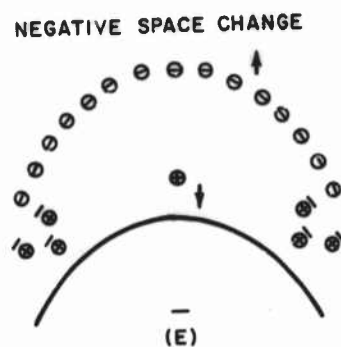


Figure 1 MECHANISM OF TRICHEL PULSE CORONA

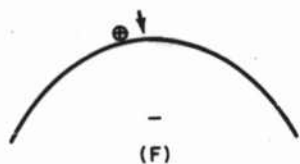


THE OUTER ELECTRONS
BECOME ATTACHED AS
O-IONS. POSITIVE ION
IMPACT ON THE CATHODE
GIVES NEW ELECTRONS AND
FRESH AVALANCHES.
(A γ_1 MECHANISM)

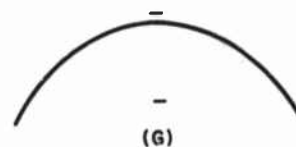


THE NEGATIVE SPACE
CHARGE HAS AN INCREASING
TENDENCY TO CHOKE OFF
THE MAINTENANCE OF THE
DISCHARGE BY POSITIVE ION
IMPACT.

↑
(NEGATIVE SPACE CHARGE)



THE DISCHARGE HAS
CEASED. THE NEGATIVE
SPACE CHARGE IS MOVING
AWAY.



A BELATED POSITIVE ION
PRODUCES AN ELECTRON.
A NEW PULSE STARTS.

⊕ POSITIVE ION
⊖ NEGATIVE ION
- ELECTRON

Figure 2 MECHANISM OF TRICHEL PULSE CORONA

production by photon impact upon the cathode (γ_p mechanism). The pulse is protracted by avalanches resulting from electrons generated by positive ions hitting the cathode (γ_i mechanism), and is choked off by the accumulation of negative space charge. The relative effectiveness of the γ_p and γ_i processes depends upon the pressure in the gas. As pressure is reduced from atmospheric, the γ_i mechanism becomes increasingly important. Figures 1 and 2 are probably applicable to a pressure of about 200 mm of mercury. At atmospheric pressure however, the γ_p mechanism is very efficient. The result is that the current pulse rises rapidly; dissociative attachment to form a high-density, quenching, negative space charge occurs quickly; and the total duration of the pulse is appreciably less than 10^{-8} sec.²¹

It would be expected that with the figure given above for pulse duration it should be possible to obtain pulse-repetition frequencies approaching or exceeding 100 mc/s. However, in the extensive work of Loeb and his colleagues,²⁴ 1 mc/s seems to be accepted as the limit for Trichel pulse-repetition frequency before breakdown of the gap occurs. On the other hand Large²⁵ using a simple point-plane arrangement, reached a frequency of 10 mc/s before sparking took place. It may well be that the limit attained is not that physically realizable, but is rather conditioned by the experimental circumstances, and in particular the practical difficulties of obtaining fields intense enough to produce copious corona, and extending over considerable dimensions. It is difficult to reproduce the field configurations of the thundercloud in the laboratory.

Some typical figures for a point in corona are perhaps enlightening. The quantum of charge for a point of 0.2 mm radius is about 10^{-10} coulomb. Thus a current of 1 μ a would correspond to a pulse repetition frequency of 10 kc/s and 100 μ a to 1 mc/s. This kind of current can be attained with potentials of the order of 30 kv in a point-plane arrangement with a gap of a few centimeters.

1.3.1 The radio-noise due to Trichel pulse corona

The distribution of the electromagnetic energy radiated by a point in Trichel pulse corona has been considered by Large.²⁵ There are three main factors involved, namely the spectrum of the individual pulse, the pulse repetition frequency F , and the degree to which the pulse repetition frequency is constant. It will be assumed that all the pulses are similar although, as will appear later, this is not always the case in practice.

Large²⁵ has shown that the amplitude distribution along the spectrum is given by the function $G(s)$

where,

$$G(s) = \left\{ \frac{\sinh \left(\frac{\Delta^2 s^2}{2} \right)}{\cosh \left(\frac{\Delta^2 s^2}{2} \right) - \cos s r} \right\}^{1/2} \left\{ S_p \right\} \quad (7)$$

In expression (7) s is the angular frequency and equal to $2\pi f$ where f is the actual frequency. The intervals between the Trichel pulses are assumed to be Gauss distributed with a mean interval of r and a standard deviation of Δ , while S_p is the spectrum of a single pulse. As a first approximation, an individual pulse may be taken as a square wave of 10^{-8} sec duration, ²¹ and with this assumption it can be shown that,

$$S_p = \left\{ \frac{\sin \frac{s}{2 \times 10^8}}{\frac{s}{2 \times 10^8}} \right\} = \frac{\sin \frac{\pi f}{10^8}}{\frac{\pi f}{10^8}} \quad (8)$$

Thus, S_p only begins to deviate appreciably from unity at a frequency well above 10 mc/s.

$$\text{The behavior of } A_s = \frac{\sinh \left(\frac{\Delta^2 s^2}{2} \right)}{\cosh \left(\frac{\Delta^2 s^2}{2} \right) - s r}$$

is more complicated. As $s \rightarrow 0$, $A_s \rightarrow 0$, while for large values of s , A_s tends to the limit of $\tanh \frac{\Delta^2 s^2}{2}$. In the intermediate region, A_s has successive maxima and minima, steadily diminishing in intensity with increasing s , but which are more pronounced in sharpness and greater in detectable number, the smaller the value of Δ . This is readily seen by expanding the hyperbolic functions in A_s . A_s may then be written as,

$$\frac{\Delta^2 s^2 + b}{2(1 - \cos s r) + c} \quad (9)$$

where b and c represent the small expansion terms of second and higher orders. It is obvious from equation (9) that the condition $\cos sr = 1$ is approximately that for the successive maxima, and that the intensity of the maximum is primarily controlled by the residual term c and will therefore be larger the smaller the value of Δ .

In figure 3, A_s is plotted as a function of s . Four scales are included referring respectively to values of r of 10^{-4} , 10^{-5} , 10^{-6} , and 10^{-7} sec; these correspond to pulse repetition frequencies of 10 kc/s, 100 kc/s, 1 mc/s, and 10 mc/s. Three curves are drawn for three values of the standard deviation Δ . All the curves tend to 1 as a limit; the curve for $\Delta = r/3$ is drawn in full; that for $\Delta = r/30$ has most of the maxima and minima and the upper envelope shown; that for $\Delta = r/300$ only has the two envelopes indicated. Figure 4 is a plot of S_p against s . Figure 5 is of $G(s) = A_s S_p$ against s for $r = 10^{-6}$; only the envelope curves are shown for the three values of Δ . Figure 6 is similar to figure 5 but for $r = 10^{-7}$ in this instance. It is noteworthy throughout how a decrease in the standard deviation produces a marked pronouncement of the maxima.

1.4 Natural Point Discharge

Point discharge from a point upon the surface of the earth into the atmosphere, under the influence of the high potential gradients associated with stormy weather, does not differ physically from the corona observed in the laboratory. Large and Pierce¹⁴ have shown that the same kind of fine structure is encountered in the two cases. There is, however, an important practical difference. In the laboratory the opposite electrode is never too far removed and the law of corona current is usually referred to voltage. In the atmosphere, on the other hand, the electrode of opposite polarity to the point (at earth potential) is within the thundercloud, and accordingly, the point discharge or corona current is usually related to the vertical electric field E_0 at the surface of the earth. The relationship that is found is of the form,

$$I = B E_0 (E_0 - S) , \quad (10)$$

where I is the current, s is the field or potential gradient at which the discharge commences, and B is a constant. Relationship (10) can be translated into a "voltage" form. The law of (10) applies to a point, at a height h (say) above the surface of the ground, and electrically connected to the earth. If E_z is the potential gradient at a height z , and V_h the potential discontinuity at the tip of the point between the point and the ambient atmosphere, then,

$$V_h = \int_0^h E_z \cdot dz , \quad (11)$$

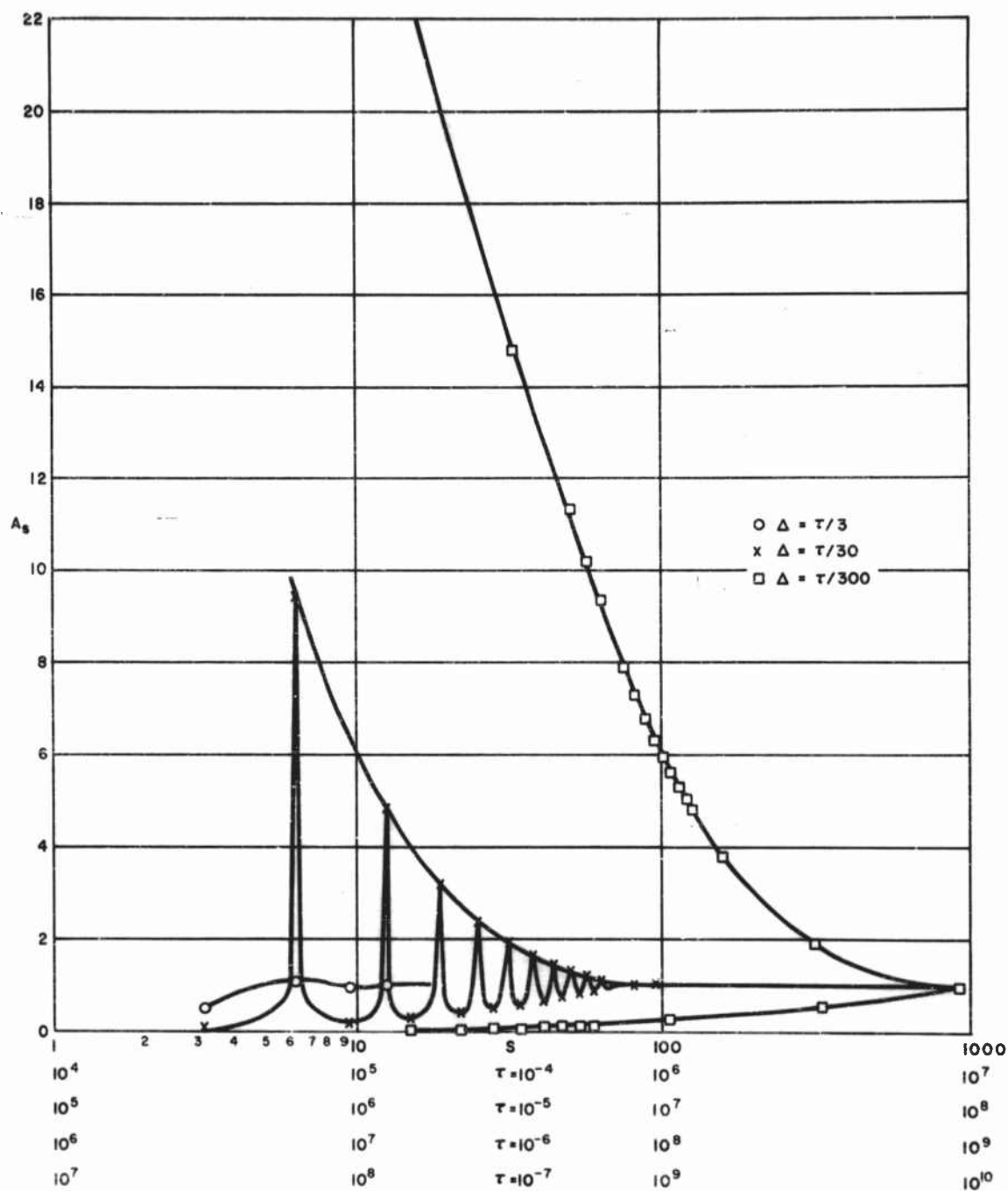


Figure 3 CONSTANT CHARACTERISTIC OF GAP A_s VERSUS ANGULAR FREQUENCY s .

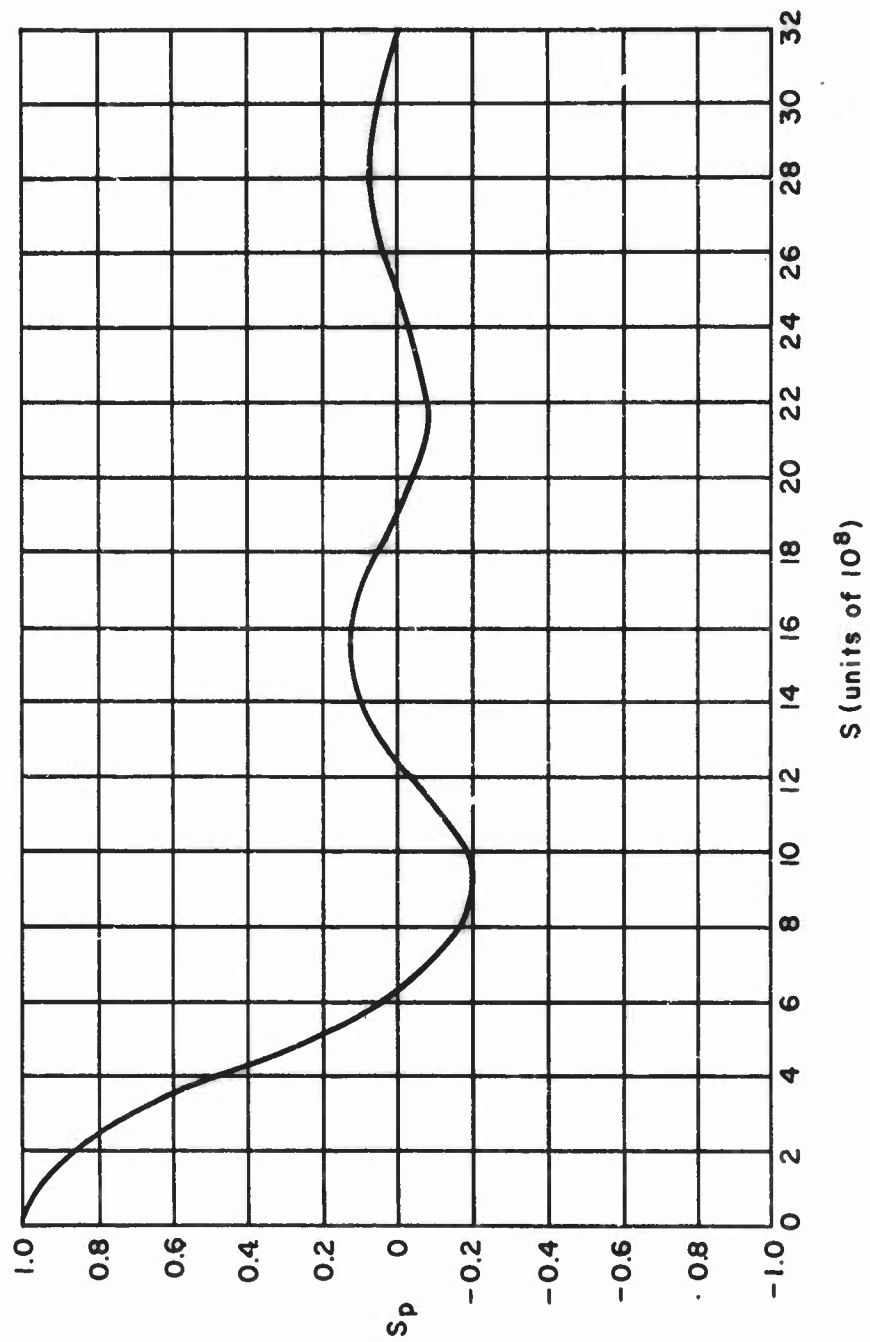


Figure 4 SPECTRUM OF SINGLE PULSE s_p VERSUS ANGULAR FREQUENCY s

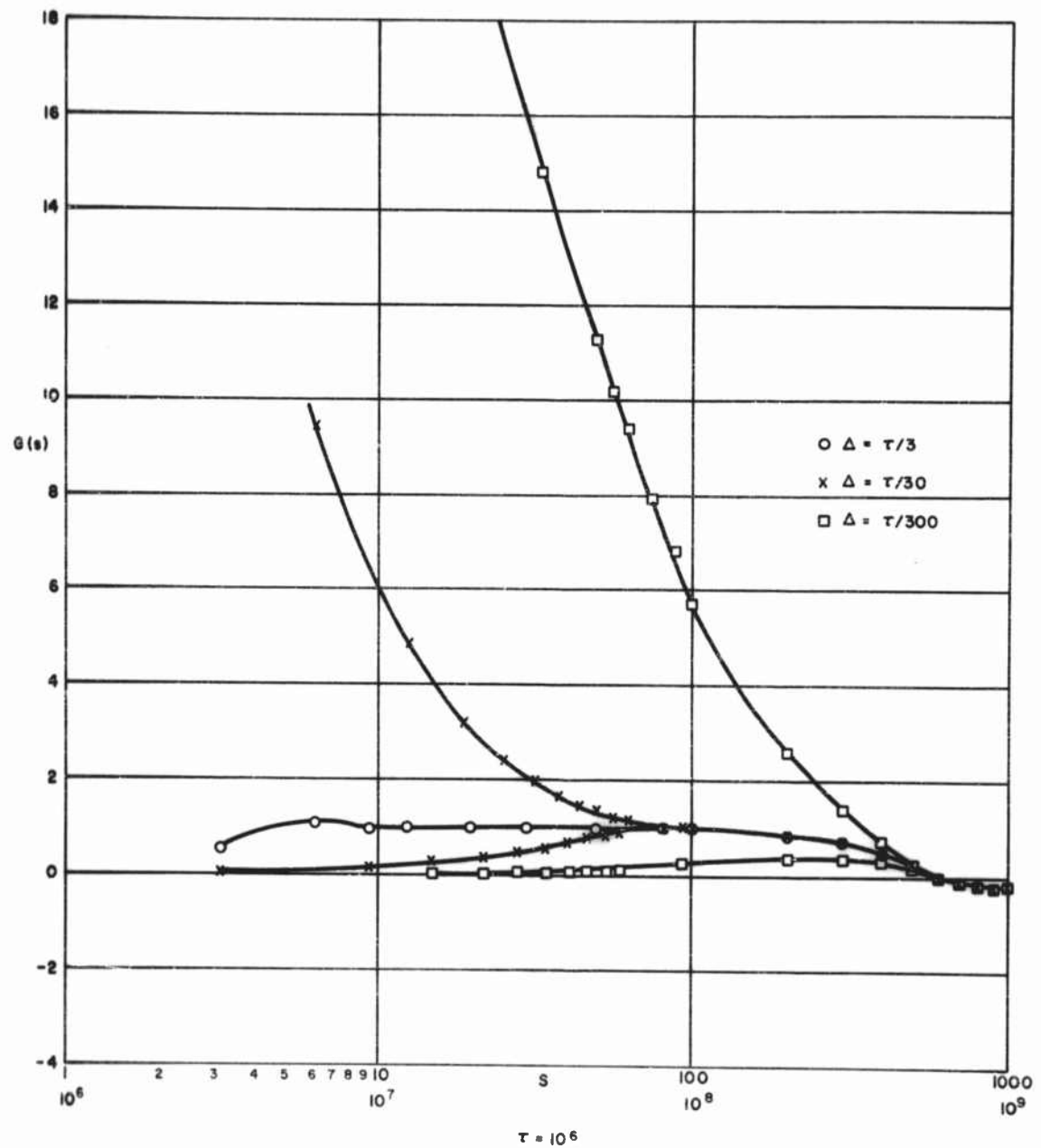


Figure 5 AMPLITUDE DISTRIBUTION $G(s)$ VERSUS ANGULAR FREQUENCY s
FOR $\tau = 10^{-6}$ SEC

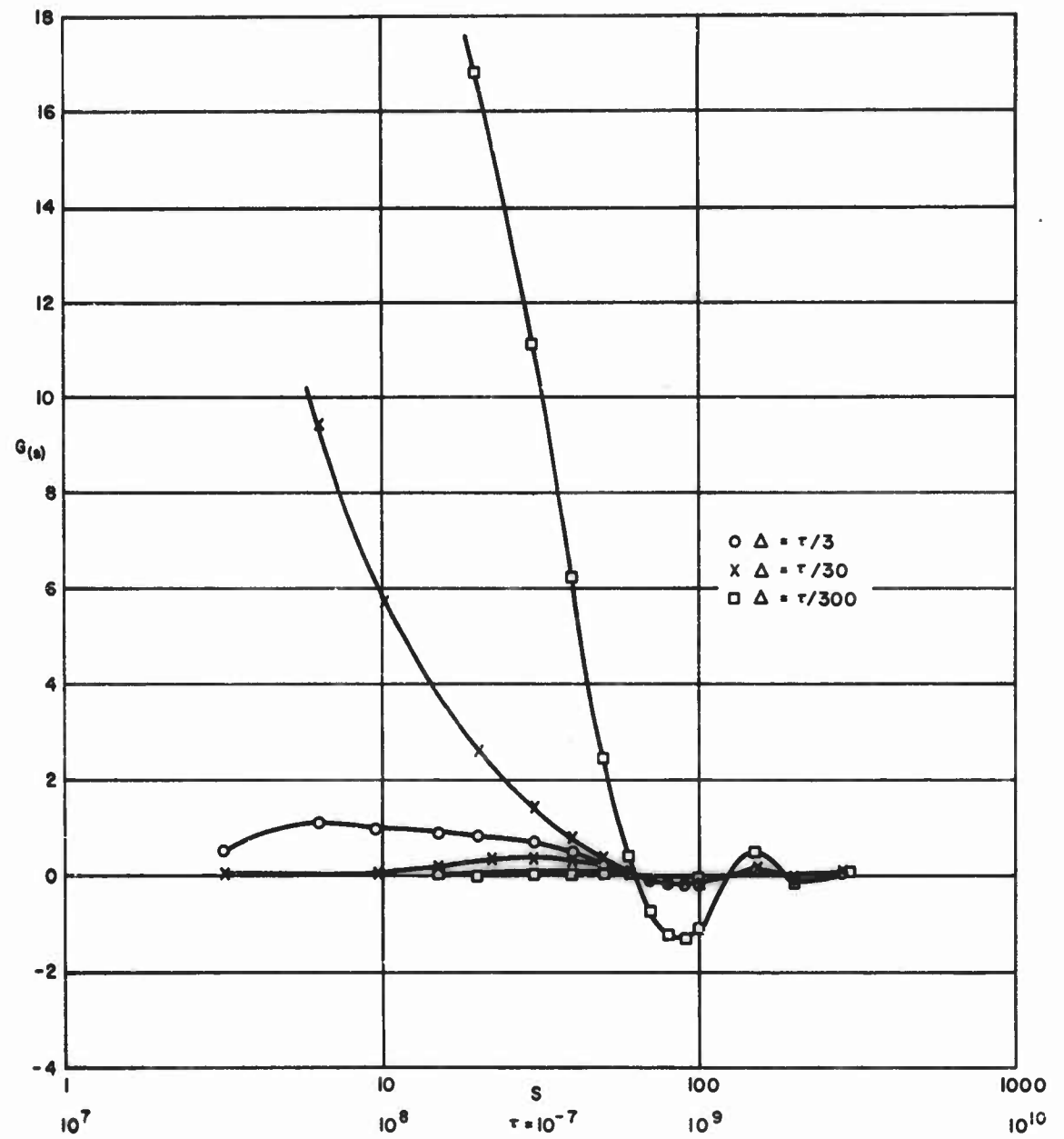


Figure 6 AMPLITUDE DISTRIBUTION $G(s)$ VERSUS ANGULAR FREQUENCY s
FOR $\tau = 10^{-7}$ SEC

or, since h is usually only of the order of a few meters, E_z is effectively constant over the distance h and equal to E_0 , so that $V_h = E_0 h$. Equation (10) may be thus rewritten as,

$$I = B \cdot \frac{V_h}{h} \left\{ \frac{V_h}{h} - S \right\} \quad (12)$$

This may be compared with expression (5).

It will be recalled that the constant A in expression (5) effectively represents the removal of space charge. In a laboratory experiment this removal is almost entirely brought about by the influence of the electric field. Under atmospheric conditions, however, another factor enters--the wind. The importance of the wind effect has been indicated by several workers, both for natural conditions^{26, 27} and in wind tunnel experiments.²⁸ The wind factor may be included by revising expression (10) so that it becomes, in an arrangement consistent with (10),

$$I = \frac{B}{k \omega} (E_0 - S) (W^2 + k^2 \omega^2 E_0^2)^{1/2} \quad (13)$$

where W is the wind speed, ω the ionic mobility, and k a constant indicative of the integrated degree to which the field near the point deviates from the value E_0 . The term under the square root sign represents the speed of dispersal of the space charge, it being assumed that the wind (horizontal) and the field (vertical) are mutually perpendicular factors. Equation (13) shows that an increase in current can be brought by a stronger wind as well as by a more intense potential gradient.

The current obtained from an artificial point mounted above the surface of the ground and exposed to atmospheric conditions, is probably the best guide to the current flowing under natural circumstances from natural points such as trees. A classic series of point-discharge experiments were carried out by Whipple and Scrase.²⁹ They used a point with a tip of radius 0.2 mm at a height of 8 m. In their experiments Whipple and Scrase did not consider the influence of wind, but the empirical relationship that they obtained can readily be modified to include the wind factor. The result is,

$$I = 2.10^{-4} (E_0 - 8) (W^2 + 4 E_0^2)^{1/2} \quad (14)$$

where I is in microamperes, E_0 in v/cm, and W in cm/sec. Below a thunder-cloud W is zero for a complete calm, perhaps 1000 under average conditions,

and 3000 in gusts. The information of Wormell³⁰ suggests 100 as an average for E_0 and 500 as the extreme value. Table I is plotted for these figures.

TABLE I
VALUE OF POINT-DISCHARGE CURRENT
(MICROAMPERES) FOR INDICATED CONDITIONS

Wind Speed (cm/sec)	0 (Calm)	1000 (Mean under T/S)	3000 (Gust under T/S)
Field (v/cm)	---	---	---
100 (Mean under T/S)	3.7	18	55
500 (Maximum under T/S)	98	106	301

If the previous value of 10^{-10} coulomb for the quantum of charge associated with a point of 0.2 mm radius is taken, then the extrapolated pulse repetition frequency corresponding to 300 microamperes is 3 mc/s. Higher values will be obtained for sharper points.

The information given in Table I is essentially for flat terrain copiously supplied with natural points. If points are more scarce there is reason to believe that the current per point will be higher. Chalmers³¹ has indicated that for a single thundercloud the total point-discharge current is controlled only by processes within the storm, the tendency being for a natural equilibrium to be established in which the charges in the cloud are constantly being destroyed by point-discharge currents and replenished by internal generation in the thunderstorm. The point-discharge current density below the storm will be approximately constant; thus the fewer the points the more current each point will have to carry.

Another factor tending to increase current is topography. Mountains lead to an intensification of E_0 and hence of I . Cobb, Phillips, and Allee,³² have reported currents of several milliamperes during thundery conditions at the summit of Mt. Washburn in Yellowstone Park. On the other hand the maximum corona currents recorded by Moore, Vonnegut, and Emslie³³ on Mt. Withington in New Mexico are only of the order of tens of microamperes, although some other remarkable corona effects have been noted by the same workers on the Mt. Withington site.

1.4.1 The ball lightning theory

The extension to Kapitsa's idea has already been outlined in section 1.1; some further simple development will be given in this section. Figure 7 represents the sequence of events in a thundercloud as it affects the discharge from a single point. Initially, in figure 7 (a), the cloud is electrically neutral but contains a mixture of positive and negative carriers of charge. These gradually separate to produce a net positive charge at the summit of the cloud and a net negative charge towards the base. The field that develops causes corona from the point to occur, thus building up a positive space charge immediately above the point. Conditions immediately prior to the flash to earth are shown in figure 7 (b). The model of the thundercloud is the simple model of $+Q$ at a height $2H$ and $-Q$ at a height H introduced by Simpson and Robinson.³⁴ The space charge is represented by $+q$ at a height z . In actual practice, the charges are of course distributed over volumes (not necessarily uniformly) rather than concentrated at particular spots, but the simple picture is adequate for an analysis designed to be illustrative but not precise. The flash in figure 7 (c) is assumed to remove the charge $-Q$ to ground, leaving the electric field controlled by $+q$ and $+Q$. The discharge strikes the earth adjacent to the point. In so doing it will produce upward streamers from any protuberances on the surface of the earth and even from open ground.^{1, 35} These streamers range in length from one to several meters. Their development is arrested by the collapse of the locally intense field, following the establishment of the conducting channel between cloud and ground. The resultant collapsed streamers are plasmas potentially able to absorb radio-frequency energy. It is probable that a discharge close to any point which it does not actually strike will generate a plasma near, but detached from, the point; the detachment results from the collapse of the original streamer and is also assisted by such influences as wind. Following the discharge, the polarity of the point with respect to the ambient air is negative. Trichel pulse discharge will therefore commence and can radiate into any nearby plasma. The pulse repetition frequency (p-r-f), will depend upon the current from the point. If a plasma is to be maintained for some seconds by the absorption of radio energy in the Kapitsa manner, the p-r-f (and consequently, the current) should be relatively constant over such a period of time. Two competing influences can possibly bring this about as is illustrated in the succeeding analysis.

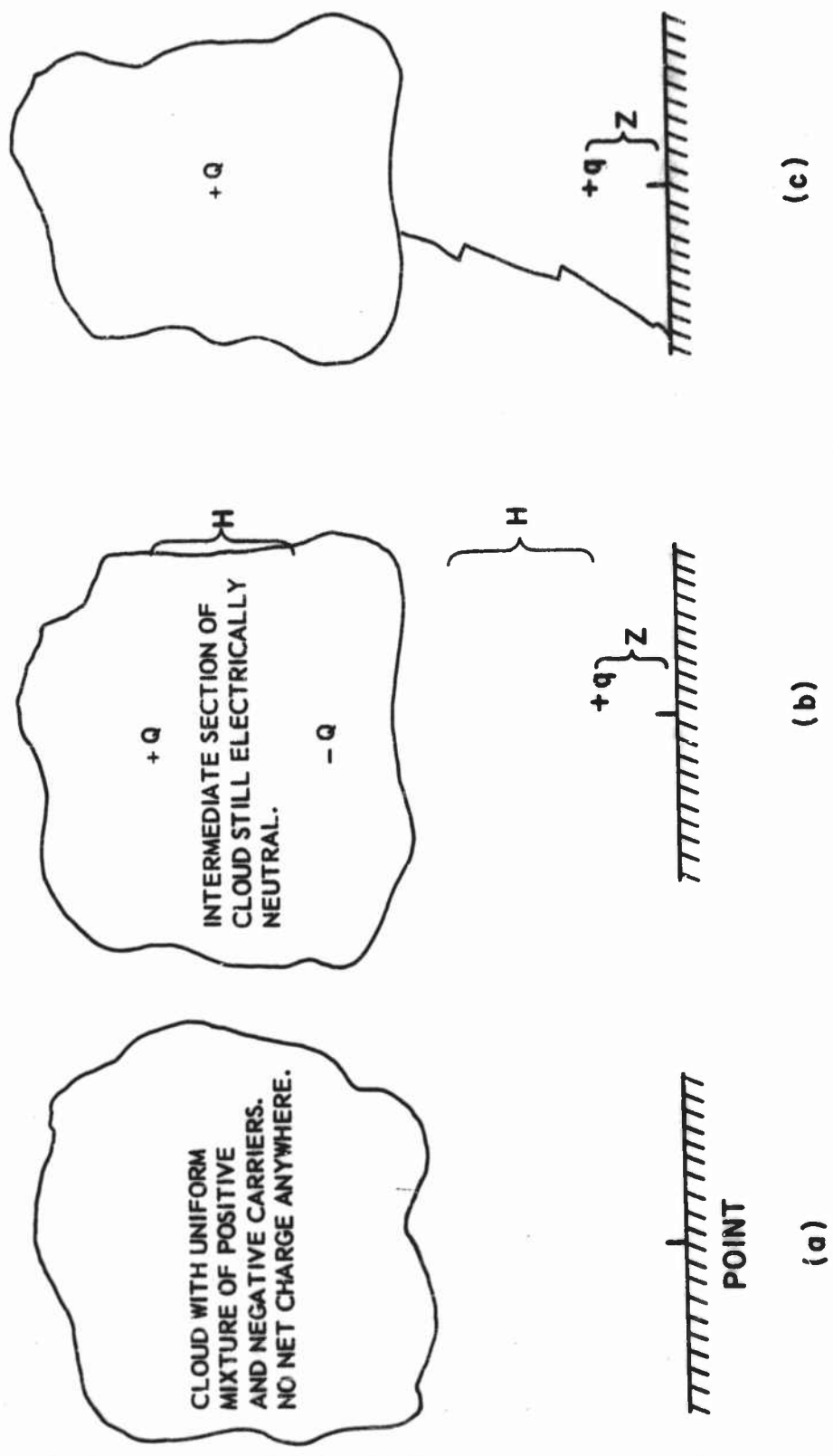


Figure 7 SEQUENCE OF EVENTS IN FLASH TO EARTH

The field E_0 at the ground at the time of figure 7 (b)* is given by,

$$E_{0b} = \frac{2q}{z^2} - \frac{3Q}{2H^2} .$$

Immediately after the flash, as in figure 7 (c),

$$E_{0c} = \frac{2q}{z^2} + \frac{Q}{2H^2} . \quad (15)$$

Some of the work of Wormell³⁰ suggests -100 V/cm and + 500 V/cm as plausible for E_{0b} and E_{0c} . Hence, $Q/H^2 = 1 \text{ e.s.u.} = 300 \text{ V/cm}$, which is consistent with the values of $Q = 30$ coulombs and $H = 3$ km; these figures in turn are not far removed from those given by Simpson and Robinson,³⁴

$$\frac{q}{z^2} \text{ is equal to } \frac{7}{12} \text{ e.s.u.} , \quad (16)$$

q and z may be estimated independently. The time between figures 7(a) and 7 (b) is of the order of several minutes (say 5); during this period the mean point discharge current is a few microamperes, (zero field to begin; 100 V/cm to terminate) so that q is of the order of 10^{-3} coulomb. The mobility of the ions liberated at the point is equal or less than the small ion mobility of about 1.5 cm/sec per V/cm. The maximum field of 100 V/cm gives a peak velocity of 150 cm/sec, but during the period of figure 7 (a) and 7 (b) the mean speed will be much less. Supposing that the time of travel of the ions is, on the average, two minutes, then 20 meters would seem a reasonable round figure value for $z \cdot q = 10^{-3}$ coulomb and $z = 20\text{m}$ gives $q/z^2 = 3/4$, which is not far removed from the $\frac{7}{12}$ value of equation (16).

Following the flash the field is dominated by q , and

$$\frac{dE_{0c}}{dt} = \frac{2}{z^2} \cdot \frac{dq}{dt} - \frac{4q}{z^3} \cdot \frac{dz}{dt} . \quad (17)$$

If the p-r-f is to remain effectively constant, I and E_{0c} must not change appreciably with time soon after the discharge. The condition for this is found by equating (17) to zero giving,

$$\frac{dq}{dt} = \frac{2q}{z} \cdot \frac{dz}{dt} , \quad (18)$$

*Electrostatic units rather than the more fashionable m.k.s., are used without apology since the ensuing relations are simpler, the problem being essentially an electrostatic one. Conversion factors are, 1 e.s.u. = 300 volts, 3 e.s.u. = 10^{-9} coulomb.

for immediately after the flash. z will change because of the motion of q under the now positive field towards the ground. Approximately,

$\frac{dz}{dt} = -\omega E_{0c}$, where ω is the mobility, and immediately following the flash, $\frac{dz}{dt} = 750 \text{ cm/sec}$. q may be considered to decay because of the continuing neutralization by the negative ions liberated at the point, and

$$\frac{dq}{dt} = -I = -k_1 E_{0c}^2 \quad (19)$$

By comparison with equation (14), k_1 in equation (19), (which is in e.s.u.), is equal to $108 \cdot 10^3$, and the L.H.S. of equation (18), with E_{0c} at 500 v/cm, is approximately 3×10^5 . The RHS with $z=20m$ and $q=10^{-3}$ coulomb is approximately 2×10^6 . Thus the agreement is at least to within an order of magnitude. This is perhaps as well as can be expected in view of the crudity and uncertainty of the calculations. Notable errors are involved in: (1) the estimates of ionic mobility which may range between the 1.5 cm/sec per v/cm characteristic of small ions and the 10^{-3} cm/sec per v/cm of large ions, and the even lower values for small droplets, all depending upon the degree of attachment involved; (2) the spatial distribution of charge and field; (3) the varying parameters for corona from different points, and so on. The analysis is, however, perhaps sufficient to indicate that the opposing influences of movement of the positive space charge toward the point and diminution of the magnitude of the space charge by the negative corona from the point, can tend, in certain cases, to produce a temporary constancy of field at the point immediately after a flash. The resultant constancy of p-r-f would be a factor on the suggested theory in stabilizing the ball lightning.

It should perhaps be pointed out that if the relaxation time for stability of the ball is long, then, even with a changing prf, there is a chance of maintenance of the ball lightning for a considerable time. Suppose the ball were of the dimensions to accept a frequency of 300 mc/s, then if the p-r-f were 60 mc/s, the ball would stabilize upon the fifth harmonic; if the p-r-f then dropped to 50 mc/s stabilization would be on the sixth harmonic. Thus in a situation of changing p-r-f, the ball might well tend to select the harmonic that would maintain its existence as unaltered as possible.

1.4.2 Necessities of ball lightning theory

It is perhaps desirable to stress some of the features that have to be fulfilled if the theory advanced above is tenable. Not all of these can be readily tested, and it is certainly beyond the scope of the present

work to carry out a complete verification. Nevertheless, the major factors are worth cataloging.

(1) Natural point discharge currents are undoubtedly a source of r-f energy at the surface of the earth. It remains to be shown that their intensity is sufficient to provide appreciable coupling into nearby plasmas.

(2) The existence of the plasmas close to the points needs to be demonstrated. Their possible preference for certain locations as a result of magnetohydrodynamic influences requires examination.

(3) The r-f signals from the corona are supposed to have line spectrum characteristics in the region of 300 mc/s. Factors favoring this behavior are:

(a) As high a pulse repetition frequency as possible.

(b) Little jitter in p-r-f, or in other words a small standard deviation in the distribution of the intervals between pulses.

(c) A short pulse duration. This influence in fact, works in two opposing ways. A short length of Trichel pulse is important for a high p-r-f. On the other hand, for frequencies approaching, and larger than, the inverse of the pulse duration, the spectrum S_p of an individual pulse becomes non-uniform (see Fig. 8). This can add to the discrete spectral nature of the complete disturbance but a counter influence is the general decrease in the amplitude of S_p .

1.5 Experimental Work

The work described in the present report is an examination of some features of Trichel pulse corona. It is directly related to (c) above but the limited extent of the experiments means that they are indecisive as regards the application to ball lightning. Two further directions, in which experimental investigations should obviously proceed, are an examination of the possibilities of feeding r-f energy at a frequency of the order of 300 mc/s by a radio link into a plasma, and a determination of the r-f spectrum for a point in intense natural negative corona on a site such as a mountain top.

The objectives of the current experiments on Trichel pulse corona were three:

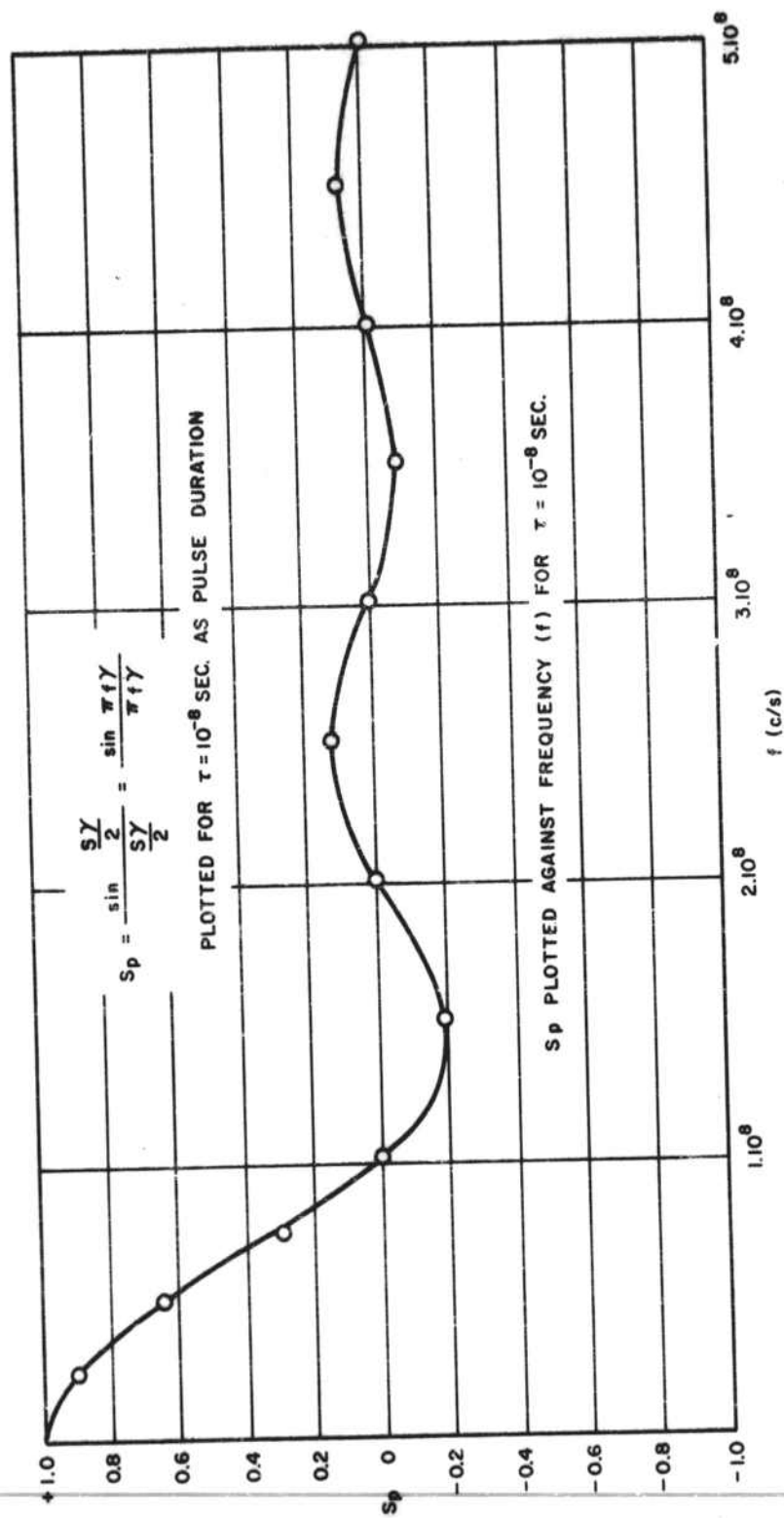


Figure 8 S_p PLOTTED AGAINST FREQUENCY f FOR $\tau = 10^{-8}$ SEC

- a. A further extimation of the highest pulse-repetition frequencies that can be attained.
- b. An accurate determination of the information, hitherto unknown, on the spread, at constant current, in the intervals between pulses.
- c. An examination of whether the spread in intervals can be reduced by the artificial injection of a frequency equal to the mean pulse repetition frequency. The injection methods would be confined to simple means and avoid any coupling by a radio link.

II. EXPERIMENTAL WORK AT BOSTON MUSEUM OF SCIENCE

In early May 1960, an opportunity arose of utilizing the van de Graaff machine at the Boston Museum of Science.

This van de Graaff machine is one of the earliest scaled-up versions of the original van de Graaff electrostatic generator. It is some 25 years old but is still under suitable conditions, capable of producing a current of 6 milliamperes at a voltage of 3 megavolts.

The immediate objective of the experiments was to determine the order of magnitude of the corona currents that could be obtained, and the pulse-repetition frequencies involved. The experimental techniques were simple. The high-voltage electrode (a large-diameter sphere) of the van de Graaff arrangement accepted the adjustable positive potential from the machine. The corona point was placed directly below the sphere and connected to earth through a microammeter, which served to indicate the corona current, and a resistance. The fine structure (Trichel pulses) in the current could be examined by tapping off, across the resistance, to an oscilloscope. Another arrangement, also used to determine the p-r-f of the Trichel pulses, consisted of an antenna mounted close to the point and picking up the radio noise therefrom. The output of the antenna was then fed into a radio receiver which could be tuned to maximum signal, thus indicating the p-r-f.

Figure 9 shows the curve obtained for corona current against voltage. It has the characteristics square-law form. Figures 10 and 11 represent the relations between corona current I and pulse repetition frequency F , and between van de Graaff voltage and F . The individual points obtained by the receiver and by the oscilloscope techniques are indicated. The agreement is reasonably good although there does appear to be a tendency, particularly at the lower frequencies, for the receiver measurements to suggest a consistently higher frequency than the oscilloscope observations at a given current or voltage. Figure 10 shows that beyond the linear region relating I and F , the p-r-f increases more rapidly than does the current. This effect, which presumably implies a reduction in the quantum of charge per pulse, was detected by Amin²¹ as occurring at reduced pressures, and is now confirmed as being present also at atmospheric pressure.

In the course of the experiments, two unexpected features were observed upon the fine structure of the discharge. The first effect, in which pulses of the opposite sign was observed indicating that the point was transiently positive with respect to its surroundings, occurred only occasionally and intermittently. It is interpreted as being due to contamination by the concentrations of space charge that inevitably form during prolonged operation of the equipment and do not dissipate rapidly by recombination. The second effect was particularly marked at the higher currents, and consisted of the occurrence of pulses of different amplitudes. At a given discharge current the pulses would be discretely distributed

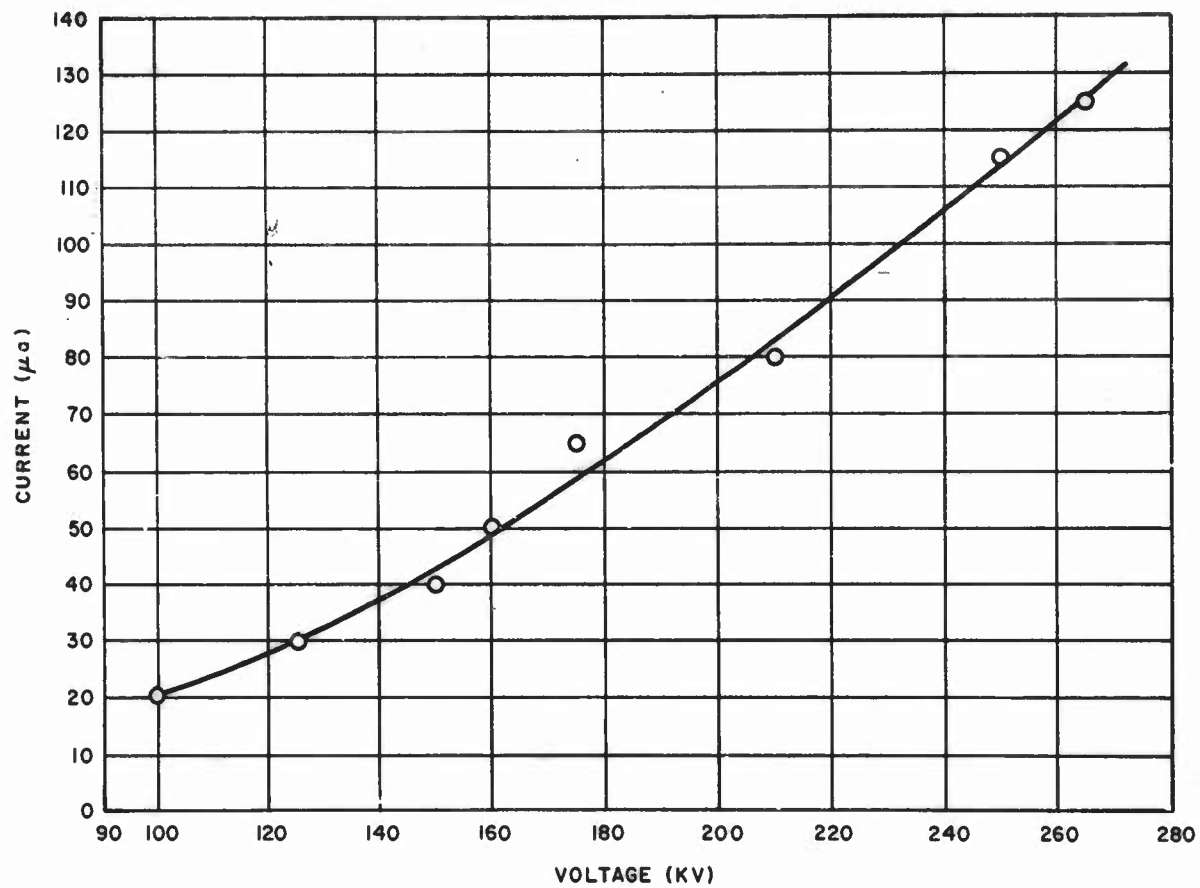


Figure 9 CORONA CURRENT VERSUS APPLIED VOLTAGE

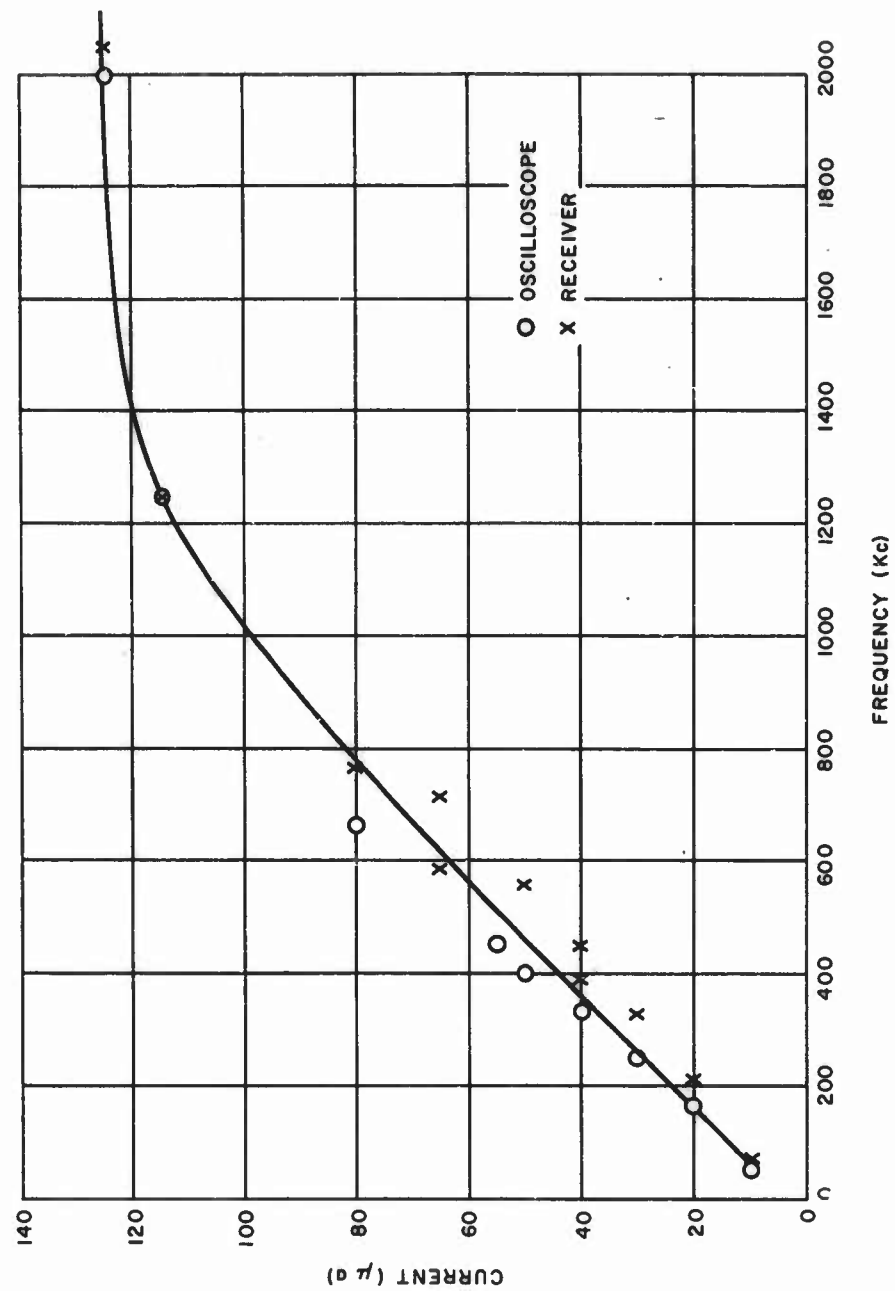


Figure 10 CORONA CURRENT VERSUS PULSE REPETITION FREQUENCY

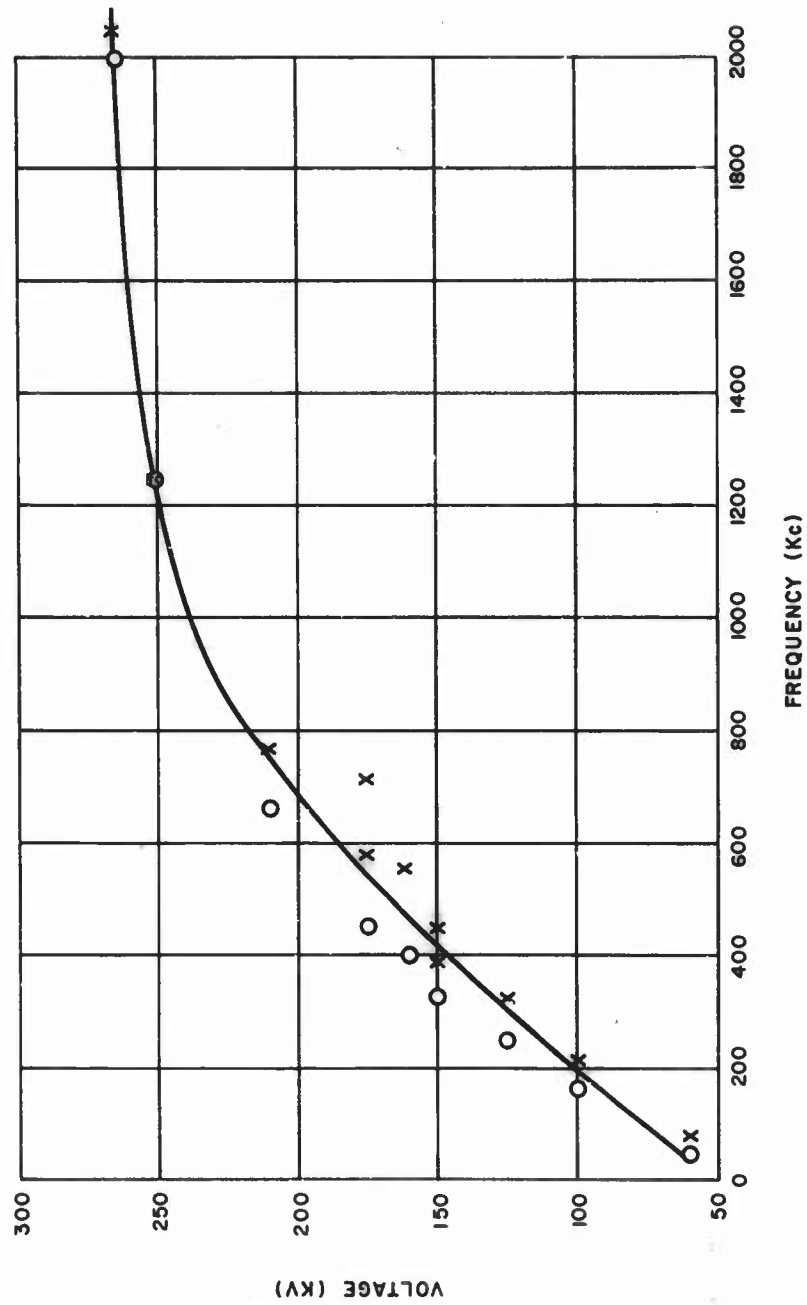


Figure 11 APPLIED VOLTAGE VERSUS PULSE REPETITION FREQUENCY

in size, but two or more families rather than one alone could often be recognized. There seemed also to be a certain independence in the pulse repetition rates for each family; this often made it difficult to assess the dominant pulse-repetition frequency. The multi-pulse behavior may well be associated with the multiple spots noted by Bandel.²²

It is felt that the experiments with the van de Graaff equipment can be pressed much farther. The maximum voltage on figures 9 and 11 is 300 kv, only some 10 percent of the peak output from the machine. The principal reasons for this conservatism were the speed with which the experimental arrangements had to be improvised and the limited time available for the performance of the work. In consequence, it was impossible to include spark arresters or diverters in the point circuitry, with the result that sparkover and resultant equipment damage was always a possibility. Considerable caution had to be used when increasing the voltage. A secondary factor, also implying such reserve, was that the van de Graaff machine itself was not functioning at optimum efficiency.

The van de Graaff arrangement simulates an extended point-plane gap and is probably as close an approach to actual atmospheric conditions as can readily be obtained artificially. It is noteworthy that currents exceeding 100 micro-amperes were obtained with the limited voltage used. Even with a relatively blunt point (radius of 0.088 mm), a pulse-repetition frequency of over 2 mc/s was reached this could certainly be increased by employing a fine wire point. It is concluded that the basic usefulness of the van de Graaff machine having now been established, a more leisurely repetition and extension of the corona experiments would be desirable.

III. TRICHEL PULSE CORONA

A routine point-plane system was employed in many of the Trichel pulse experiments. Figure 12 is a diagrammatic representation of the main features of the arrangement normally used. The point is mounted at a distance, d , from the plane that can be adjusted. The plane is the high-voltage electrode, and the point is earthy being connected to ground through a microammeter which serves to read the corona current, and a resistance. The voltage appearing across the resistance, during discharge, is fed to an oscilloscope so that the fine structure of the corona can be examined. A moving film camera is arranged so as to photograph the screen of the oscilloscope, and thus to obtain permanent records of the pulses for further analysis. A panoramic spectrum analyzer was used to examine the spectral content of the Trichel discharge. In this type of analyzer, several of which were employed with differing frequency ranges in the course of the experiments, the instrument sweeps in frequency and an amplitude content against frequency is directly displayed upon the screen of the cathode-ray tube. The d-c high-voltage generator supplies voltage of either polarity to the point-plane gap, the magnitude of the voltage (up to 30 kc) being measured by a voltmeter across the generator. An additional a-c voltage superimposed upon the d-c supply may be fed from an oscillator to the plane by means of condensers. Two condensers were normally used in series with high resistances R across each capacitor in order to equate the voltage drop; this procedure was necessary because single capacitors of high enough voltage rating were not immediately available.

Figure 13 represents some routine curves of corona current I against voltage V across the point-plane gap. The curves were obtained during preliminary experiments. They are for a series of separations (d) between the point and the plane, and for both voltage polarities, but the same point, conical with a tip radius of 0.088 mm, was used in obtaining all the curves. The behavior is conventional. The I - V curves have the general form of expression (5), and the changes in the curves for the different values of d are as anticipated.

3.1 General Features of the Pulsed Corona

As the voltage V is increased from zero, corona current I commences at a finite voltage V_s , as is indicated by relation (5) and confirmed by the experimental curves of figure 13. V_s is not very sharply defined. It is constantly fluctuating within a restricted range because of continually changing surface conditions at the point. In consequence, near onset the discharge is irregular. The current is carried by Trichel pulses of constant amplitude but the pulse repetition frequency is far from stable and varies between wide limits. With a further increase in current and voltage the Trichel pulses become well established; they continue to be of uniform amplitude and the regime is linear with a direct proportionality between

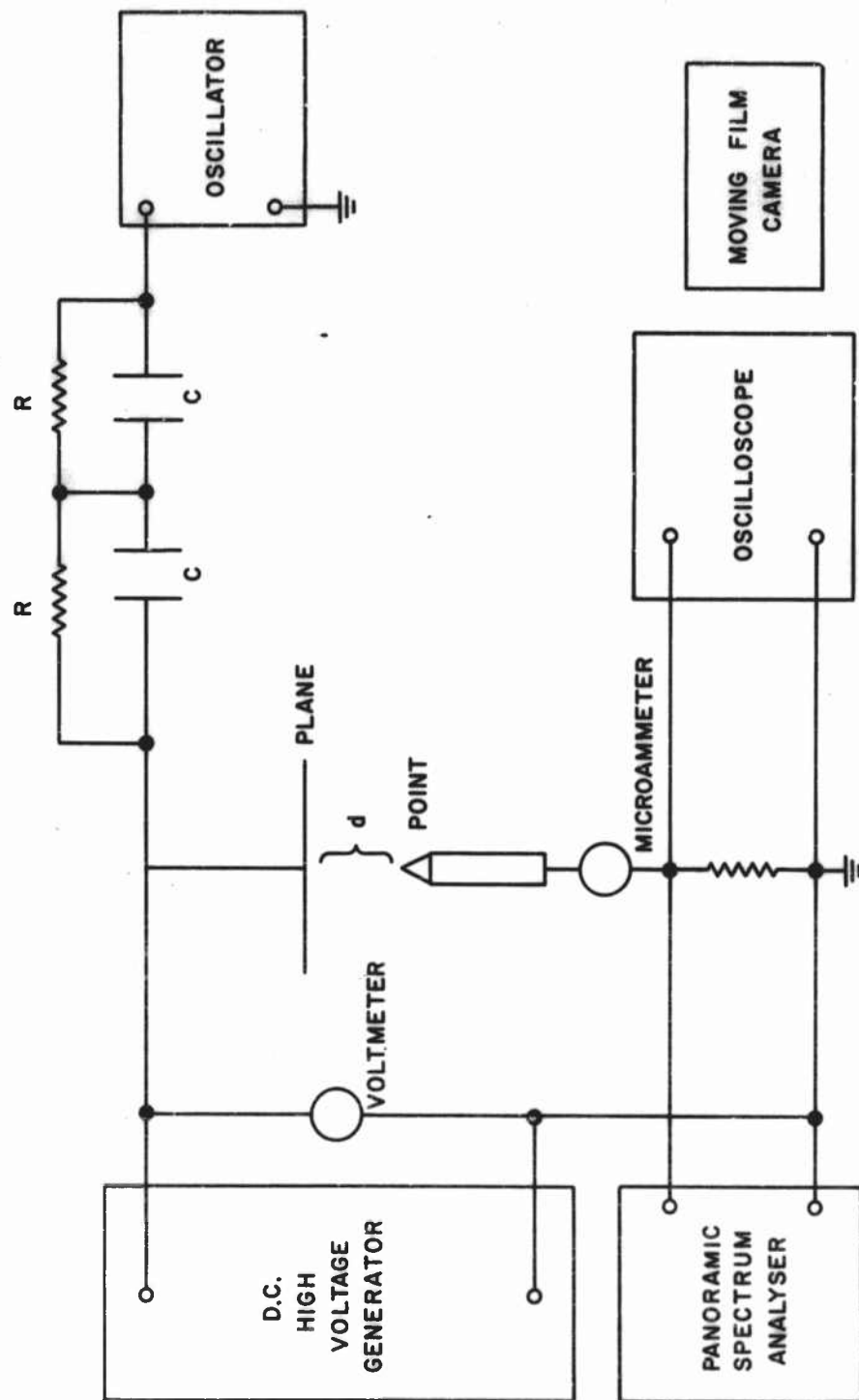


Figure 12 SCHEMATIC DIAGRAM OF EQUIPMENT

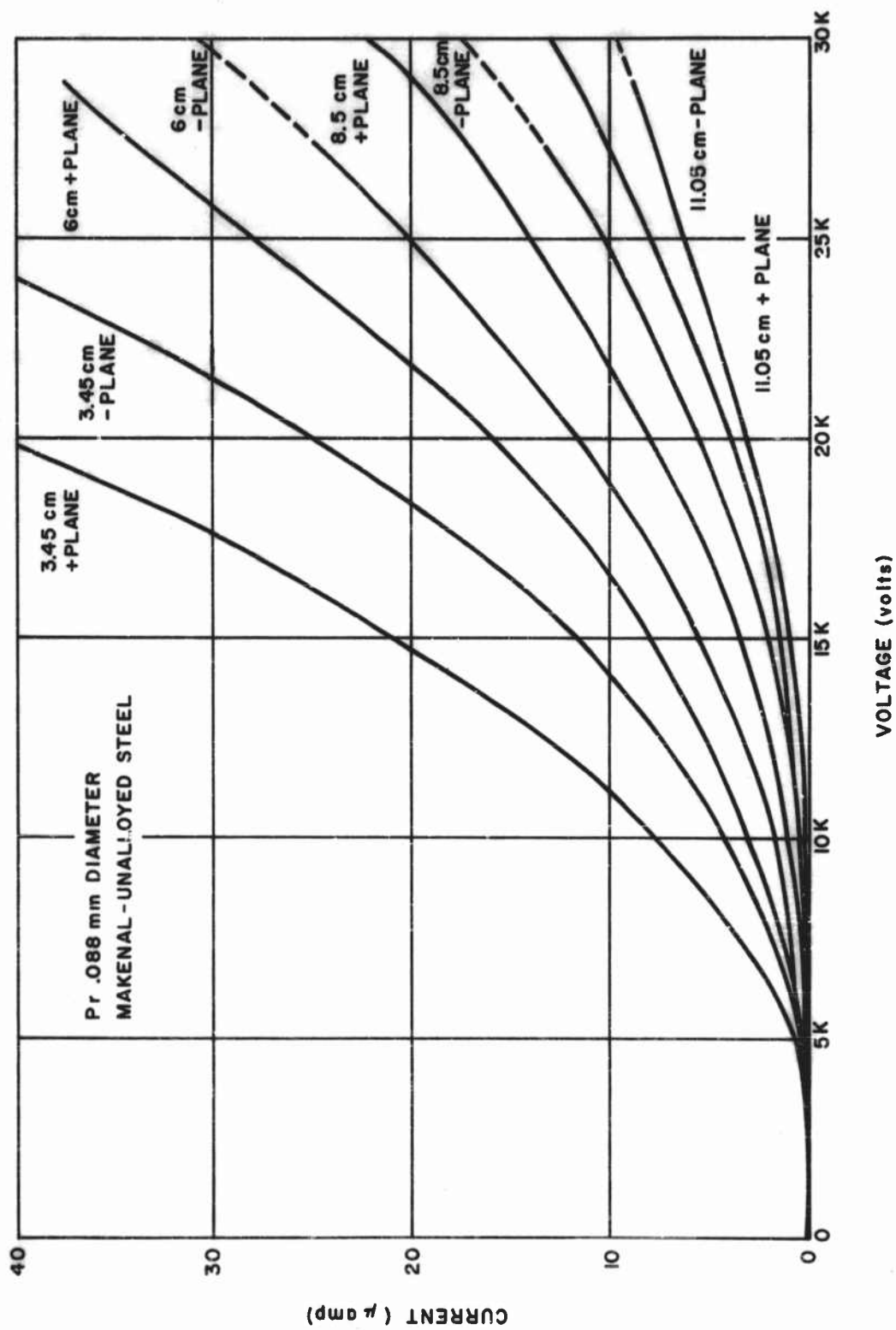


Figure 13 CORONA CURRENT VERSUS APPLIED VOLTAGE FOR DIFFERENT
POINT-PLANE SEPARATIONS

current and p-r-f. If the voltage is increased still more, the discharge often becomes of the pulseless Townsend type in which the negative space charge does not exert sufficient influence to choke off the corona periodically and thus the Trichel pulses are inhibited.

So far the phenomena described in the preceding paragraph are identical with those indicated by other investigators. However, there are three important general respects in which the present work differs from or extends previous conclusions.

Firstly, it has been found that if the voltage is raised while the discharge is in the Townsend regime, breakdown does not usually follow, but instead there is a return to Trichel pulse corona at a voltage considerably less than that required for sparkover. The pulse size is now much larger than that present before the intervening pulseless stage, so that although the current has increased, the pulse-repetition frequency is appreciably smaller than the p-r-f immediately preceding the Townsend interregnum. This sequence, with increasing voltage of onset; i. e., Trichel pulses, Townsend pulseless discharge, and larger Trichel pulses, is normally the simplest that is observed. It can often be more complicated with two or more intervening Townsend stages, while the Townsend stage may last only over a very limited range in voltage.

A second important feature that has been continually noted is the simultaneous occurrence of families of Trichel pulses, the pulses of each family being of uniform size but the amplitude differing from family to family. This effect is particularly marked for the Trichel pulse region beyond the intervening Townsend stage. Here it is common for three sizes of pulses to be present in the discharge. The usual behavior is that immediately following the Townsend regime Trichel pulses of only one amplitude are observed; with increasing voltage, however, a second and then a third family enter, and following the entry of a new family, those originally present maintain their activity undiminished. Multiple families are also sometimes apparent in the Trichel pulse region after onset. The multiplicity is more pronounced at the higher voltages approaching the transition to the Townsend regime, but is rarely as marked as for the Trichel pulses beyond the Townsend stage.

Thirdly the behavior of the pulse-repetition frequency for a given voltage setting is of very considerable interest. For simplicity the phenomena are best investigated when there is only one family of pulses present; this usually implies working in the lower-voltage Trichel region. The jitter of the p-r-f can be conveniently examined in two ways. The first is to use the panoramic analyzer; the second to employ an oscilloscope presentation continuously triggered by the pulses, with a sweep time corresponding to some ten times the mean interval, τ , between pulses. The degree to which

the pulse intervals are non-uniform is then readily revealed by the extent of the non-superposition, particularly towards the end of the trace, of the successive triggerings. When the discharge, at a constant point-plane voltage, is studied in either manner, it is obvious that normally there is an appreciable spread in the distribution of the intervals between pulses. Not infrequently, however, there is a startling stability which may last for up to several seconds. The successive oscilloscope triggerings are almost exactly superimposed, the maxima upon the panoramic analyzer become immensely sharpened, and many harmonics of the fundamental p-r-f are discretely identifiable. It may be conservatively estimated that this transient stability corresponds to a decrease of the standard deviation in the distribution of pulse intervals by a factor of at least ten. No feature has been observed as correlated with this fleeting natural acquisition of stability in the discharge, but it is believed that the most plausible explanation would involve micro-changes in the emissive and other properties of the surface of the point.

Much of the transitional behavior between Trichel and Townsend discharge, and of the incidence of multi-sized pulses, was clarified by telescopic observation of the points during corona. Three kinds of points were employed:

- a. Conical spikes of tip radius 0.088 mm, made of unalloyed steel, and not especially polished.
- b. Fine wires (silver-plated copper wire), snipped to give points of some 0.044 mm radius.
- c. Surgical needles of stainless steel (iron-nickel alloy), highly polished, and with a tip radius of 0.038 mm.

It was discovered that the transition, with increasing voltage, from Trichel corona to a pulseless Townsend discharge with a subsequent return to Trichel corona, was most commonly observed with the conical spike. Both spikes and wires often produced, simultaneously, pulses of different sizes, and this occurrence was associated with the presence of multiple glows. The glows additional to that at the tip were usually, but not invariably, at roughnesses or kinks along the shank adjacent to the tip. The surgical needles normally produced the classical Amin²¹ behavior, with increasing voltage, of constant size pulses and a steadily rising p-r-f. There was also a decrease in the amplitude of the pulses as a preliminary to the advent of the pulseless discharge. Even with the needles, however, multi-sized pulses were not infrequently observed.

As is further indicated in the following section, the behavior of the points may be generalized by stating that a single point has an increasing tendency to behave as a multiple collection of points as the ambient electrical field

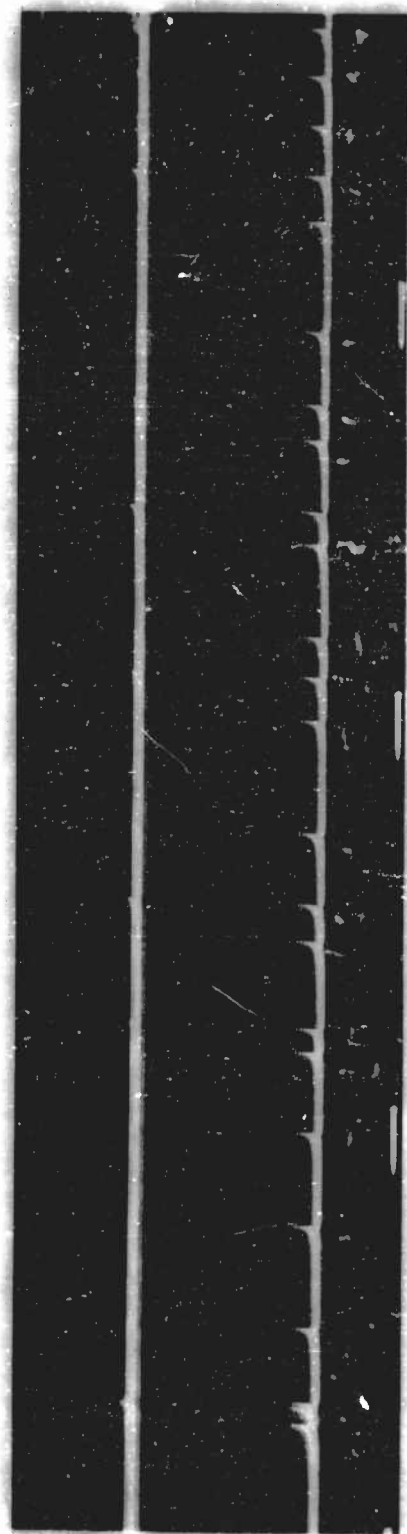
increases. The additional discharges will have, for preferred sites, any inhomogeneities such as kinks or roughnesses, spots with changed surface state, and so on. Occurrence of an additional discharge can relieve the electrical stress and thus, on occasions, prevent sparkover immediately following a pulseless stage. Multiple-point behavior will be more readily attained for unpolished rough points (as will normally be encountered in nature) than with such points as surgical needles.

3.2 Simultaneously Occurring Families of Pulses

These families of pulses have already been mentioned in Section II and discussed in Section 3.1. The present section deals with the properties of the families in somewhat more detail.

The behavior is well illustrated in figures 14, 15, and 16. These were obtained by employing a technique found to be extremely useful in the study of the discharge over a wide range of currents. Referring to figure 12, the voltage is first adjusted so as to obtain the maximum current that it is intended to study. The oscilloscope displays the fine structure of the discharge, and the moving film camera is ready to photograph the screen of the oscilloscope. Immediately the camera is set into operation; the high-voltage supply is switched off, with the result that the voltage across the point-plane gap decays, and with a time constant controlled by the values of the capacitors in the supply and the leakage resistance across the capacitors. As the voltage decays, the current diminishes. If necessary, the time constant of the decay can be adjusted so that a convenient length of record is obtained. It is desirable to measure the changing corona current at the same time that the variations in fine structure of the pulses are being examined. This is conveniently done by using a very rapid-acting electronic switch of the input to the oscilloscope; the switch alternates between an input indicating the formation of the pulses and a second input representing the integrated d-c corona current.

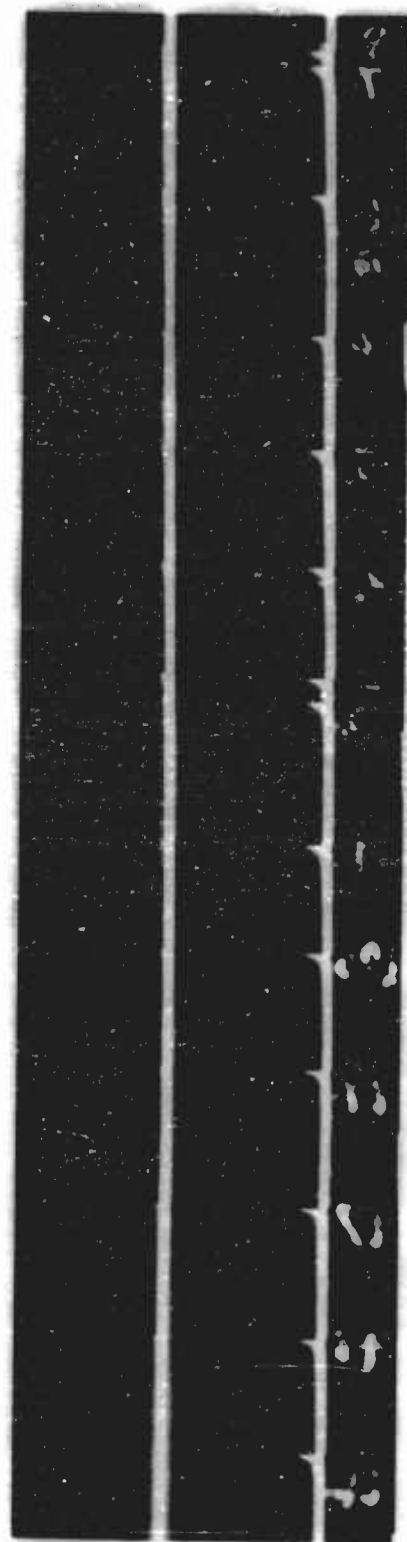
Figures 14, 15, and 16 were all obtained by the decay method described above. The figures are sections of the same record and all lie within the higher-voltage Trichel pulse regime above the Townsend discharge region. The point used was conical in shape with a tip radius of 0.088 mm; the material was unalloyed steel; and the gap width was 3.5 cm. On all three figures the sense of time increasing is from right to left, as is shown by the sharp rise of the pulses and their more gradual tailing off (this tail is largely a function of the circuitry). Timing markers at intervals of 60c per sec are on the base of each record. Two traces are visible upon the figures, these being obtained by the use of the electronic switch. The lower trace shows the individual Trichel pulses (the gaps in the pulses are produced by the electronic switch) and their baseline is fixed in position; the upper trace is a measure of the corona current and gradually moves downwards as the current diminishes so that the separation of upper and lower traces is an indicator of the current magnitude.



TIME ↑

TIME →

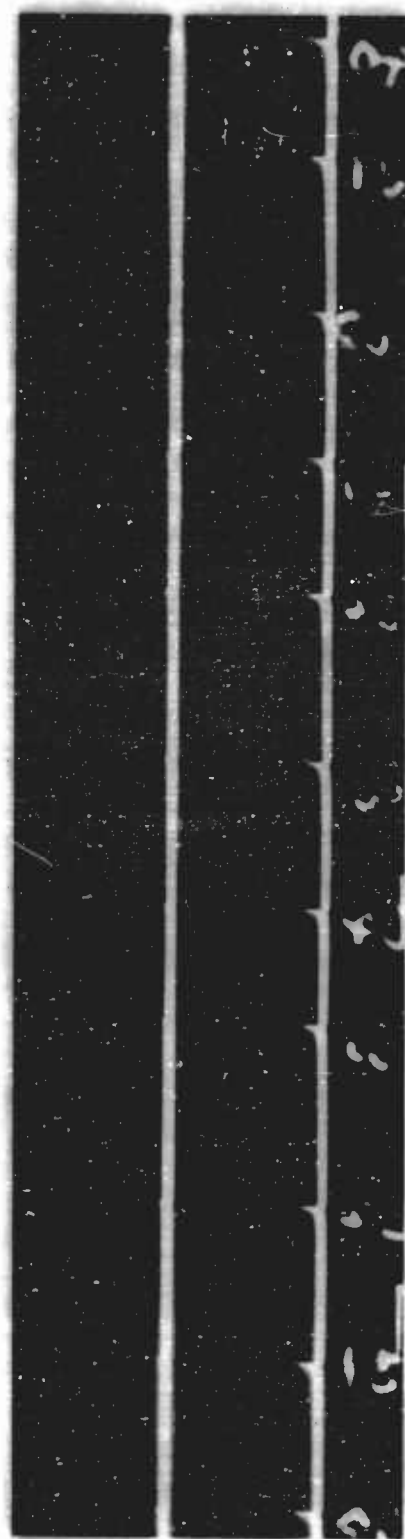
Figure 14 MULTI-FAMILY TRICHEL PULSES



TIME ↑

TIME →

Figure 15 SMALL AND MEDIUM TRICHEL PULSES



TIME ———→

TIME ———→

Figure 16 SMALL TRICHEL PULSES

Figure 14 was at a current of about 37 microamperes. Three families of Trichel pulses can be noted and may be described as of large, medium, and small amplitude; near the left-hand end of the record individual examples of each of the three families appear almost superimposed. By the time figure 15 is reached, the current has fallen to 33 microamperes; the large pulses have disappeared, but the families of small and medium pulses remain. Figure 16 represents a further drop in corona current to 28 microamperes; by now the medium pulses have also vanished and only the small pulses are left.

A plot of the time intervals between successive pulses is very revealing upon the characteristics of multi-family Trichel pulse discharge. In figure 17 three quantities have been plotted from the record of which figures 14, 15, and 16 are sections. The abscissa of figure 17 is the number of the pulse; these numbers are chosen in the reverse order of their occurrence on the decaying mechanism, with respect to time, so that the last pulse detectable on the record is Number 1, the penultimate pulse is Number 2, and so on. The three plots against the number of the pulse are corona current, the time between successive pulses, and the amplitude of the pulses. The current graph is a smooth curve. The points for pulse amplitude are reasonably uniform for pulses of small number (there is an inherent scatter due to the gaps produced by the electronic switch), but with increasing number, deviations to medium and large amplitudes become more and more common. A somewhat similar behavior is noted for pulse intervals; the scatter of the points is limited for small number pulses, but very low values begin to appear above pulse number 150, and become increasingly prevalent thereafter. There is an obvious association between large pulse amplitudes and small pulse intervals.

The clue to systematizing the behavior is evident from figure 14. Here although the pulses appear irregular, if the separate families of small, medium, and large are regarded as entirely independent, it can be seen that the large pulses are evenly spaced, as are also the medium and the small. Accordingly the data represented on figure 17 was re-examined. Pulse intervals between small pulses were measured ignoring the medium and large, and the same procedure (*mutatis mutandis*) followed for the medium and large. The results are plotted on figure 18. It is apparent that the onset of each family of pulse occurs at a definite value of corona current, and that subsequently the conventional Trichel pulse behavior applies to each separate family with a smooth increase in pulse-repetition frequency (decrease in pulse interval) as the corona current rises.

The conclusion is irresistible; i. e., several spots are active simultaneously on the point.²² Each spot is responsible for one family of pulses and figure 18 indicates that the spots have little influence upon each other. The families are independent rather than neighborly. Such independence may

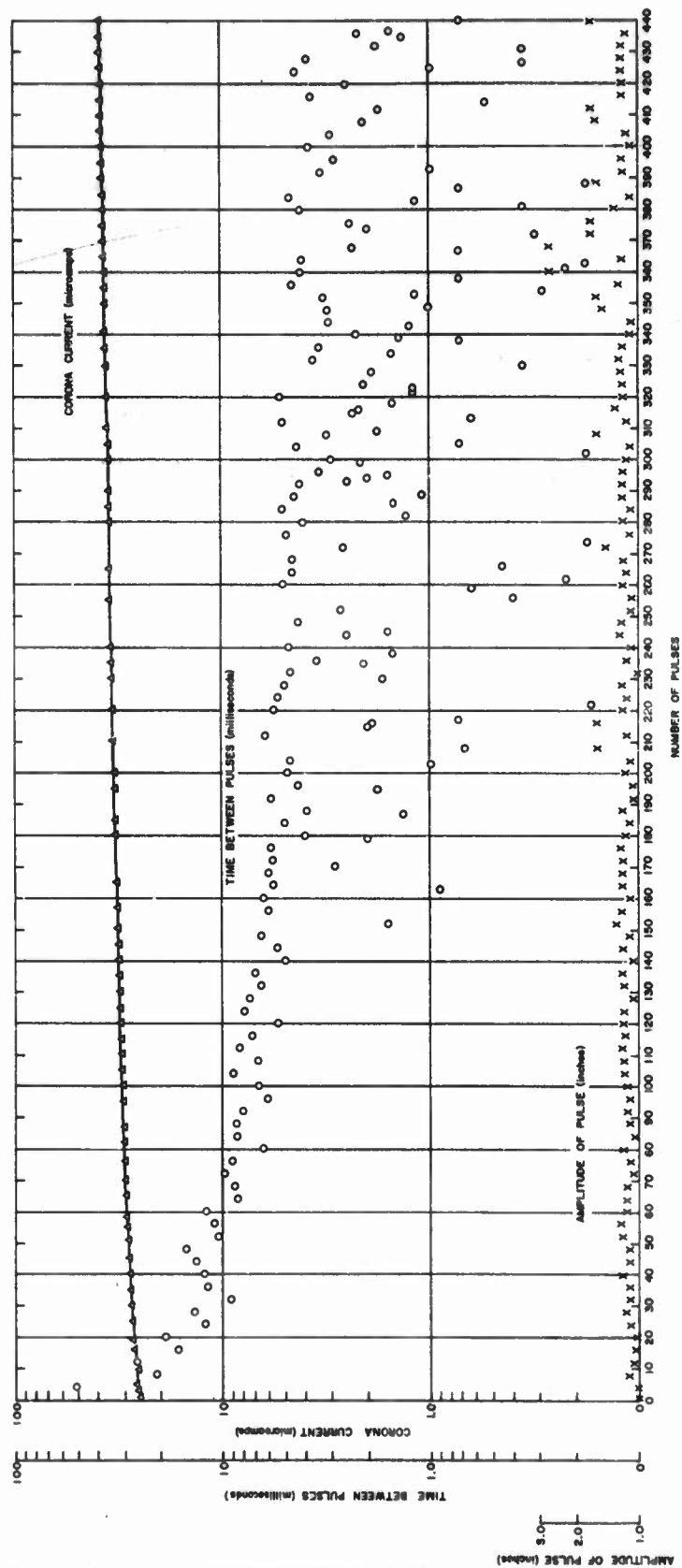


Figure 17 CHARACTERISTICS OF MULTI-FAMILY TRICHEL PULSES

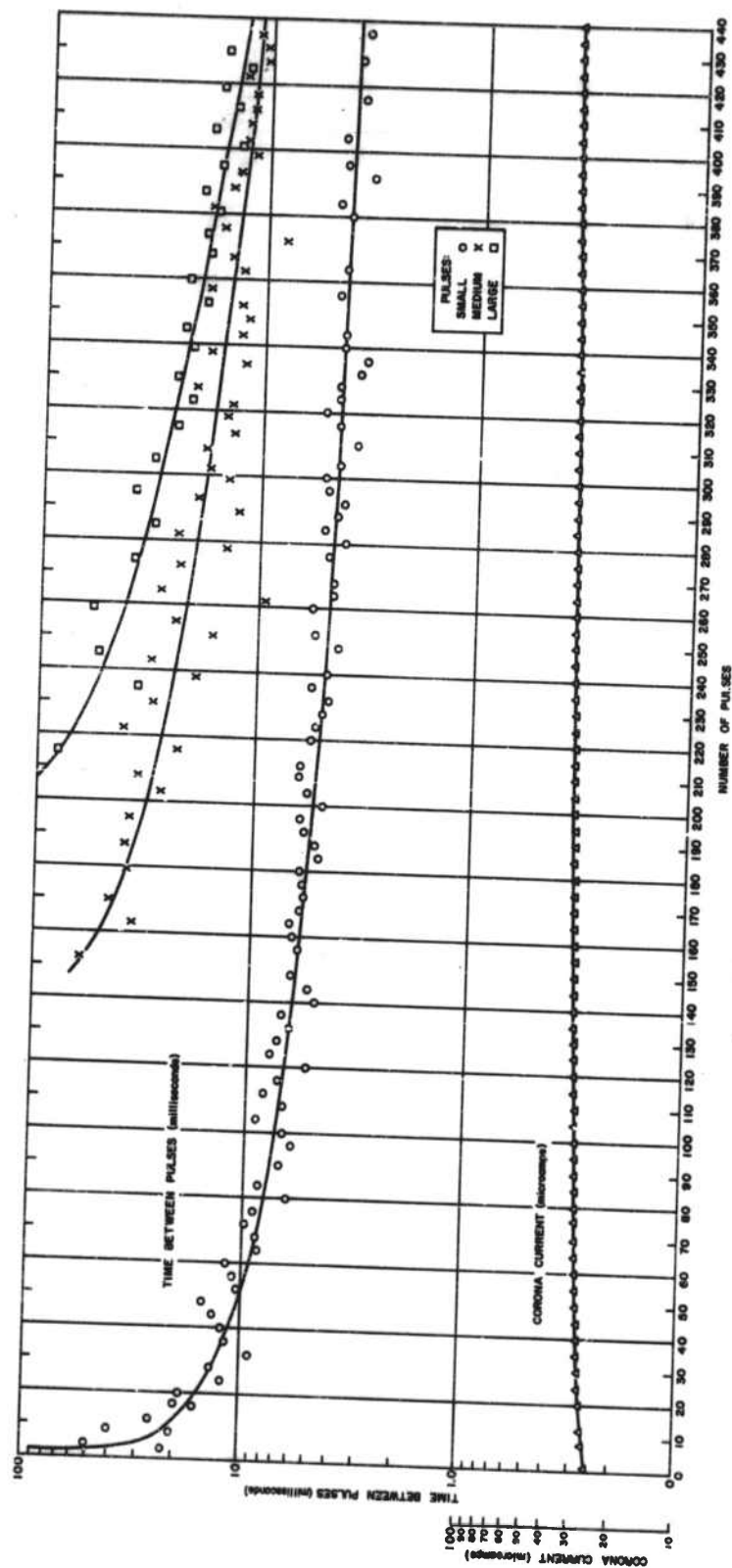


Figure 18 FAMILY PULSES CONSIDERED SEPARATELY

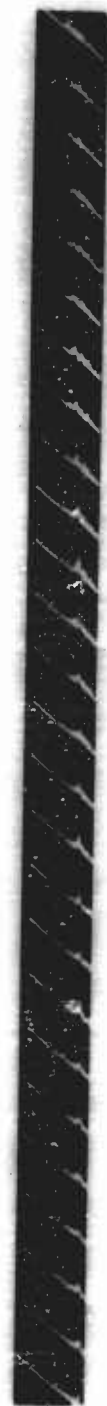
arise from a spacing brought about, as indicated by Loeb,³⁶ by a mutual repulsion of discharges. This feature is particularly evident in the uniform separation of the individual glows for negative d-c corona from a cylindrical wire.^{37, 38} It is more probable, however, that, as indicated in the preceding section, surface roughnesses and spots with particular emission characteristics will determine the preferred sites for the individual discharges.

A frequency spectrum was obtained from 85 kilocycles per second down to 350 cycles per second. This was done with the panoramic spectrum analyzer of figure 12. A short film-strip enlargement shows the results in figure 19. As the applied voltage decays, the characteristic Trichel pulses decrease in frequency. The peak, gradually moving from right to left represents the changing frequency. It can also be observed that the peak has a smaller amplitude as it approaches the 350 cycle point.

3.3 Standard Deviation of Pulse Intervals

Among the objectives listed in Section 1.5 is the obtaining of precise knowledge upon the spread of the individual pulse intervals in Trichel corona from the mean, or, in other words, the determination of the standard deviation Δ . In the present work the required information was derived experimentally by the obvious, if somewhat laborious, method of (1) analyzing a record against time of the Trichel pulses; (2) measuring a sufficient selection of the pulse interval times; and (3) applying the necessary statistics. Attention had to be confined to comparatively low-pulse-repetition frequencies, mainly because of the difficulties of obtaining suitable records for pulse intervals of small duration, and also because of the associated problem of measuring the individual intervals with a time resolution sufficient to enable meaningful values of the standard deviations to be obtained. However, knowledge of the standard deviations at low frequencies only, is at least a better guide to the behavior at higher frequencies than no knowledge at all.

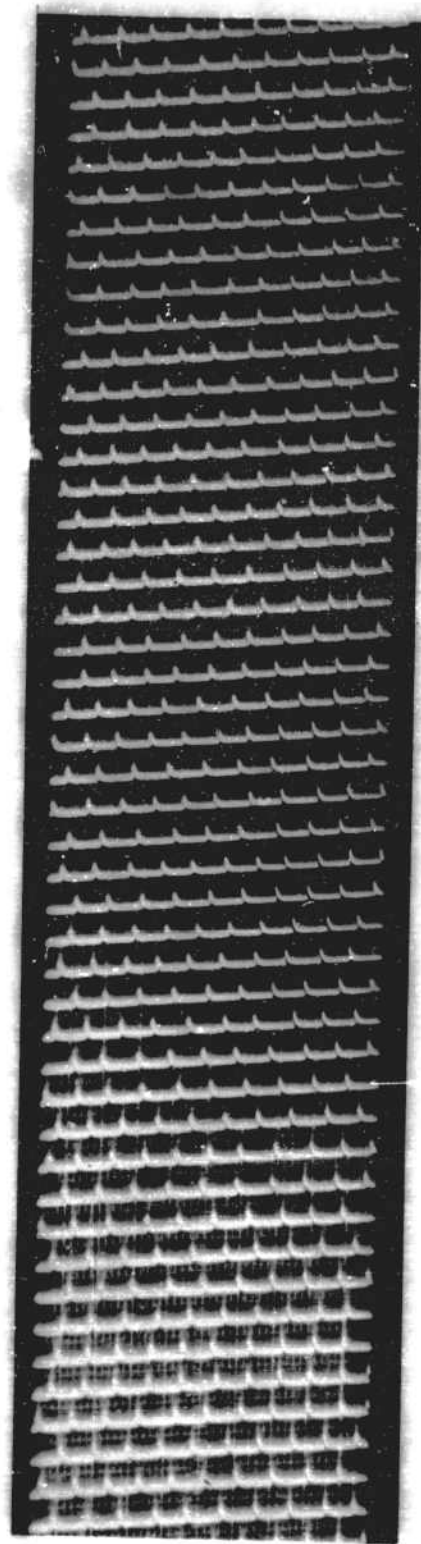
Figure 20 is a record of the individual pulses for a mean pulse-repetition frequency of about 10 kc/s. A point of tip radius 0.044 mm was used at a separation of 3.5 cm from the plane. The material of the point was silver plated copper wire. A voltage of 4.2 kv was applied to the point-plane gap, with a resulting corona current of 0.5 microampere. In order to achieve maximum time resolution for a given expenditure in film, figure 20 was obtained by using the combination of a vertically moving film within the camera and a horizontal time sweep across the face of the oscilloscope with the pulses superimposed as vertical deflections. The sense of time increasing is from left to right along the sweep, and from bottom to top along the record; the total time of the sweep is 1 millisecond. The comparative regularity of the pulse intervals is well shown on figure 20. Figure 21 represents the panoramic analyzer record obtained simultaneously with figure 20.



TIME ↑

TIME →

Figure 19 FREQUENCY SPECTRUM (85 kc/s - 350 c/s)



TIME ↑

TIME →

Figure 20 TEN kc/s PULSES



TIME →

↑ TIME

Figure 21 PANORAMIC ANALYZER DISPLAY (10 kc/s)

Again there is a combination of a horizontal sweep with a moving film, but in this instance the sweeps across and back are executed at the same speed and there is no rapid fly-back. The scan of the analyzer was adjusted to be from 0 to 20 kc/s, and the time taken to cover this range was 1 second. Figure 21 is an excellent graphic illustration of how the major frequency response is concentrated near the center of the sweep at the basic p-r-f of about 10 kc/s. The next peak in agreement with the kind of theoretical analysis given in Section 1.3.1, occurs at the end of the scan and corresponds to the harmonic at 20 kc/s of the p-r-f.

A selection of the pulse intervals appearing upon the record, of which figure 20 is a section, were measured. The total duration of the record was 1.5 seconds, and five portions of the record (each comprising one hundred consecutive pulses) were examined. The sections were chosen at the beginning of the record, one quarter of the way along, at the center, at the three quarters point, and at the end of the record, respectively. For each section histograms were constructed showing the distribution of the pulse intervals. These results are given on figure 22. A histogram for all the intervals is also included. The standard deviation, Δ , is about 8 percent of the mean pulse interval, \bar{r} . There is not much evidence of systematic changes in Δ for the different portions of the record, but there is a significant sharpening of the distribution for the second of the chosen intervals as compared with the others. There is also a tendency for an increase in the mean value along the record, the average for the final batch of a hundred pulses being appreciably larger than that for the first hundred.

Figure 23 is a record of the individual pulses for a mean pulse-repetition frequency of about 20 kc/s. In this case, an applied voltage of 4.9 kv produced a corona current of 0.9 microampere. Figure 24 is the corresponding 20 kc/s analyzer record. It operates on a frequency band of 10 kc/s to 30 kc/s.

Figure 25 is a histogram similar to figure 22. The standard deviation, Δ , is 9.3 percent of the mean pulse interval \bar{r} . The mean appears to be fairly constant for all 500 pulses.

3.4 Stabilization of Trichel Pulse Discharge

One of the main objectives of the present work was to see if the spread of the intervals between pulses in the natural Trichel corona could be diminished by the injection of a stabilizing frequency equal to the average pulse-repetition frequency. The problem might be described as the synchronization of an erratic relaxation oscillator by an applied oscillation.

The first attempts to achieve synchronization employed a sinusoidal waveform generator. The generator voltage was applied to the point side of the

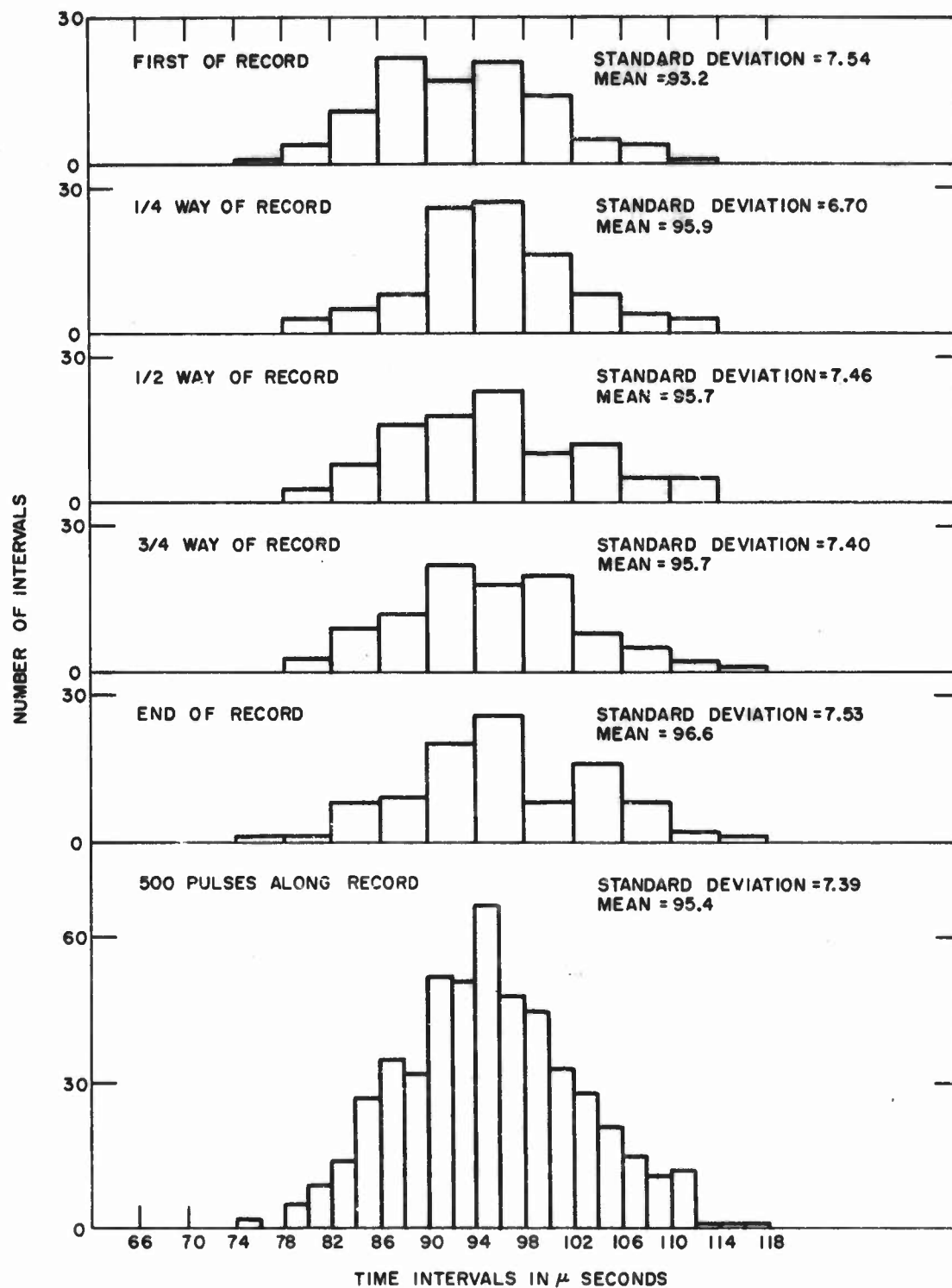
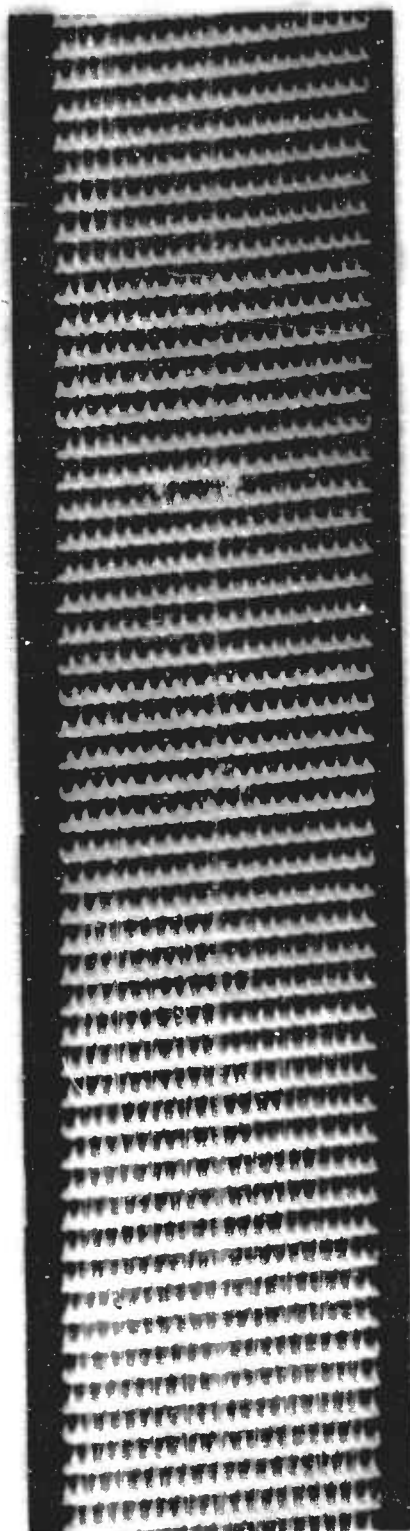


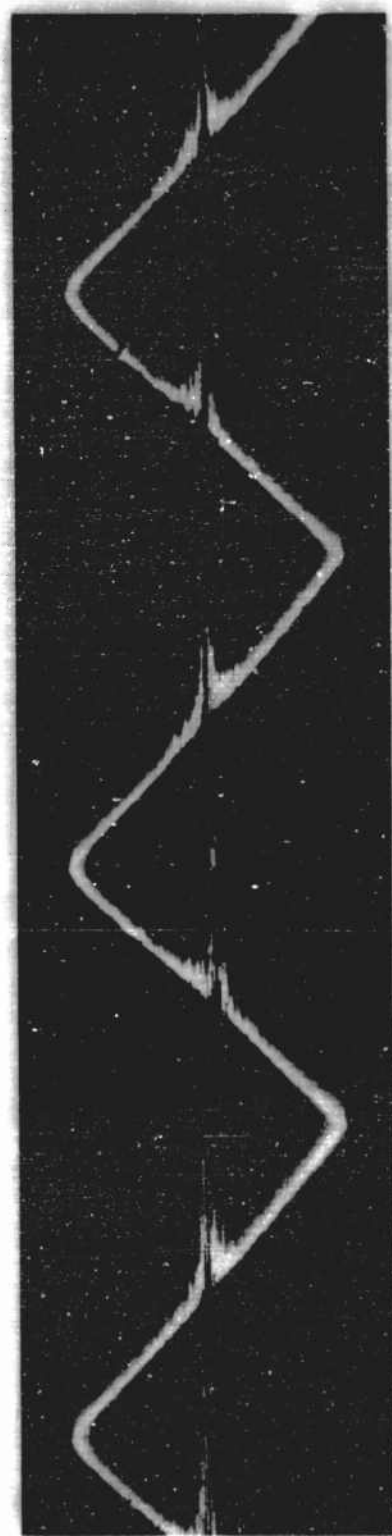
Figure 22 HISTOGRAM OF PULSE INTERVALS (10 kc/s)



↑
TIME

TIME →

Figure 23 TWENTY kc/s PULSES



TIME ↑

TIME →

Figure 24 PANORAMIC ANALYZER DISPLAY (20 kc/s)

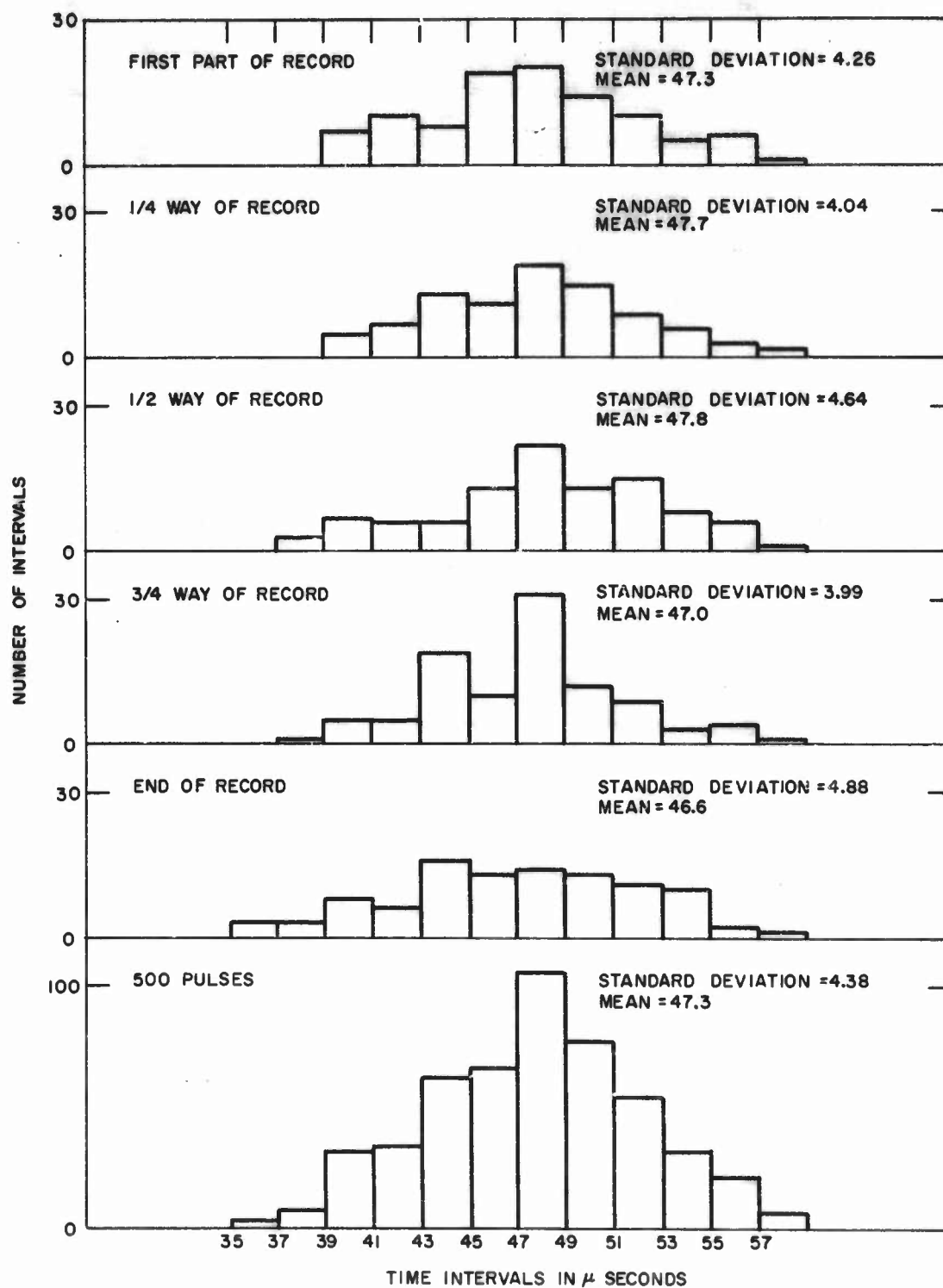


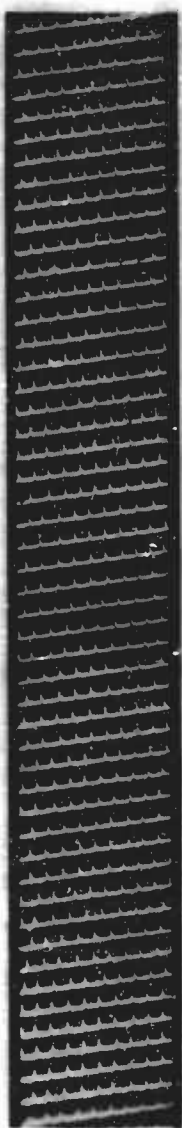
Figure 25 HISTOGRAM OF PULSE INTERVALS (20 kc/s)

gap. Injection was made in turn at all the obvious places; these included (see Fig. 12) at the point, in parallel with the oscilloscope and panoramic spectrum analyzer, and at various tapings along the resistor across the oscilloscope. Several methods of applying the generator voltage were used; these included direct d-c connection, injection through blocking capacitors, and so on. No success in improving the stability of the Trichel corona was achieved by any of the techniques utilized. In fact the tendency was, if anything, in the opposite sense; application of the stabilizing voltage usually made the discharge more irregular.

Injection into the plane or high-voltage side of the gap was then investigated, the sinusoidal oscillation being applied through blocking capacitors as indicated on figure 12. A step-up transformer was found to be useful in increasing the voltage of the sinusoidal oscillation. The general technique employed was identical with that used for the application to the point side of the gap. A corona current is first established from the point; the mean pulse-repetition frequency assessed from the indicators on the screens of the oscilloscope and spectrum analyzer. The sinusoidal generator is then set to this frequency, the sinusoidal voltage is injected, and any reduced jitter of the p-r-f determined visually from the responses of the spectrum analyzer and oscilloscope in the manner outlined in Section 3. 1.

The results obtained with injection into the plane side of the gap were much more promising than when the voltage was applied at the point electrode. Remarkable success was achieved upon one occasion when a striking improvement in stability was apparent upon the application of the impressed voltage. The stability was maintained for several hours, and whenever the applied sinusoidal voltage was removed, the corona reverted to comparative irregularity. However, in spite of numerous attempts, the same degree of success could never be repeated on subsequent occasions. Several times the application of the synchronizing voltage brought about an improvement in the stability of the discharge, but this was never as marked as in the one special instance.

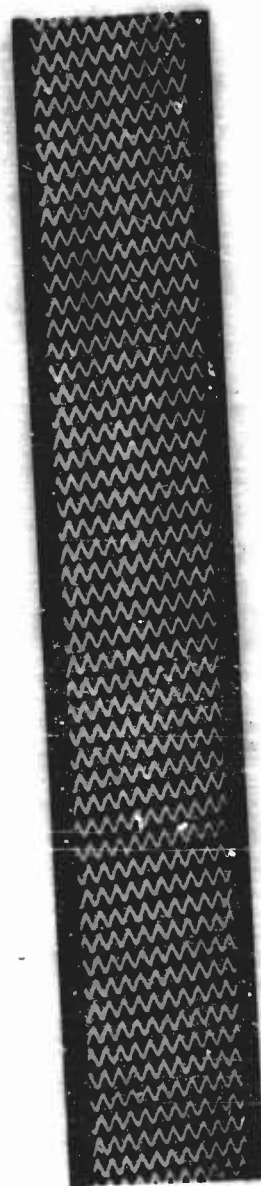
Figures 26 to 29 refer to this particular example. Figure 26 shows the pulses before the application of the sinusoidal stabilizing voltage, the d-c voltage generating the corona being 3.20 kv. Again the combination of a time sweep and a moving film is used, the sense of time increasing being from left to right along the records and from bottom to top. Figure 27 represents the response following the application of a stabilizing sinusoidal signal of 85 volts to the plate. There is sufficient pick-up of the sinusoidal waveform so that the record of figure 27 has the oscillation with a superposition of Trichel pulses; these can be seen riding upon the crests of the waves and are well synchronized to the positions of the crests. For added clarity figures 28 and 29, which represent enlarged sections of the records on figures 26 and 27, are also included. All the records were obtained with wire point of 0.044 mm radius and of silver-plated copper material; the point-plane gap was set at 3.5 cm.



TIME ↑

TIME →

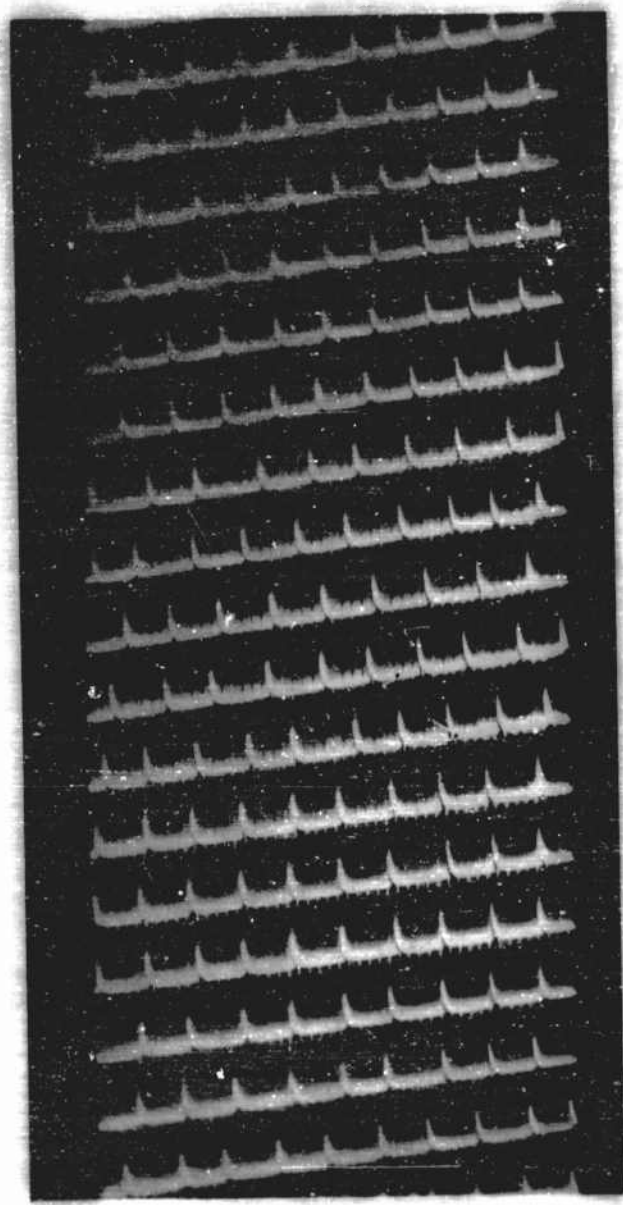
Figure 26 TRICHEL PULSES (10 kc/s)



TIME ↑

TIME →

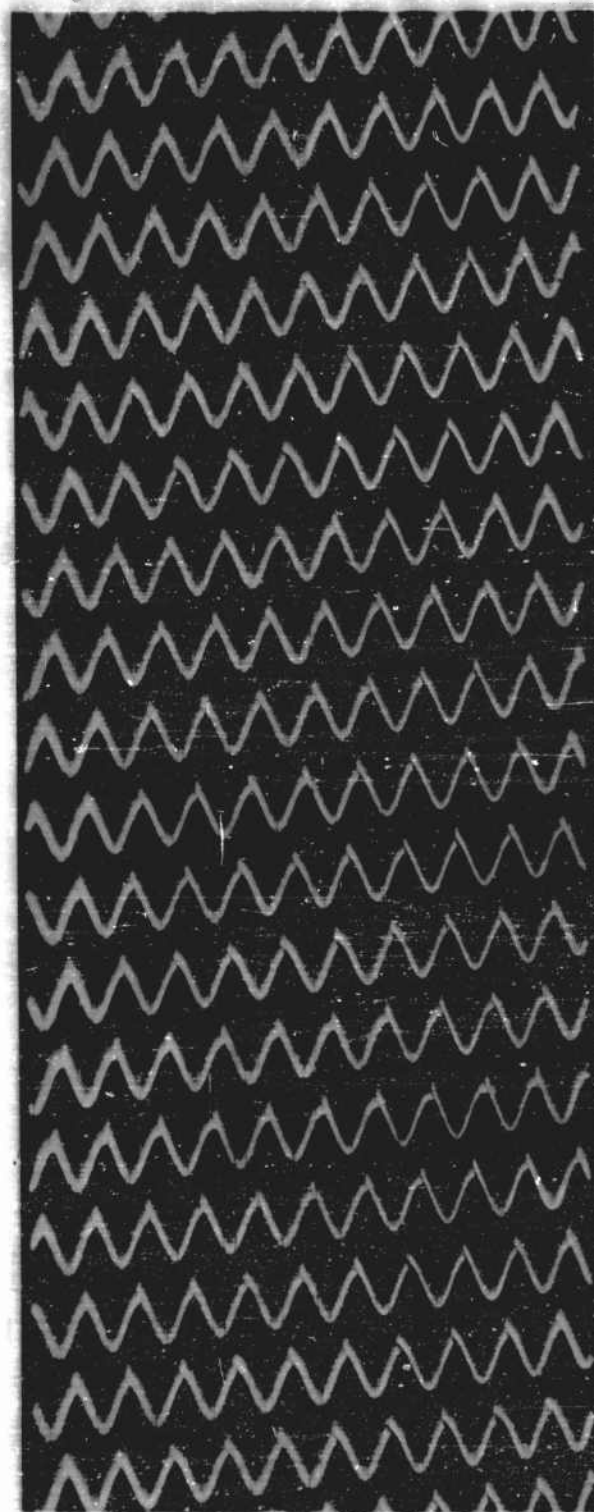
Figure 27 SYNCHRONIZATION OF 10 kc/s TRICHEL PULSES WITH 10 kc/s SINE WAVE



↑
TIME

TIME →

Figure 28 ENLARGED SECTION OF FIGURE 26



TIME ↑

TIME →

Figure 29 ENLARGED SECTION OF FIGURE 27

The intervals upon the records with and without the applied synchronizing voltage were analyzed in the manner indicated in Section 3.3. As before, five sections were chosen, each containing one hundred intervals. The results in the form of histograms, are represented on figures 30 and 31 for unsynchronized and synchronized states, respectively. It is obvious that the application of the sinusoidal voltage has effected a great improvement in the stability of the pulse frequency. An interesting feature is that the mean pulse intervals at 104.4 microsecond and 95.8 microsecond are significantly different between the two states; in other words there seems to have been a locking in of the Trichel pulses to the applied oscillation.

Figure 32 is a schematic diagram of the equipment used in one of the attempts to stabilize the corona discharge. This method was similar to that utilized in the previously mentioned successful stabilization of the discharge, except that an increase in sinusoidal generator voltage was accomplished by replacing the step-up transformer with a two-stage amplifier. A phase shifter was added at the output of this amplifier to insure that the sinusoidal generator be in phase with the corona discharge. Figure 33 is a record of the results. As may be noted, total stabilization of the Trichel pulses of a 10 kc/s mean pulse-repetition frequency was not achieved.

An impressed waveform of a sinusoidal character is basically an ineffective way of achieving synchronization. Square or saw-tooth waves are far more efficient, and accordingly further experiments were conducted using these kinds of waveforms.

3.5 Current-Frequency Relationships

Much information was acquired, during the course of the work, confirming the general relationships between current and Trichel pulse-repetition frequency. Figures 34 and 35 are typical of some of these data. They show the interdependence of V , the applied voltage, I , the corona current, and F , the p-r-f, for the discharge from a fine wire with a tip radius of 0.044 mm. P-r-f's are indicated for the two sizes of pulse that were noted during this corona. The first appearance of the small pulses was coincident with the onset of the corona; the initial generation of the medium pulses occurred at a much higher voltage. In each instance a reasonable straight line can be taken as relating I and F .

Another graph between I and F is shown on figure 36. This was obtained using a surgical needle of tip radius 0.038 mm, the surface of which had been pitted by repeated usage at high currents. Figure 36 has a general straight line relationship but the great scatter of the points, reflecting the inherent instability of corona discharge from an imperfect surface, is noteworthy.

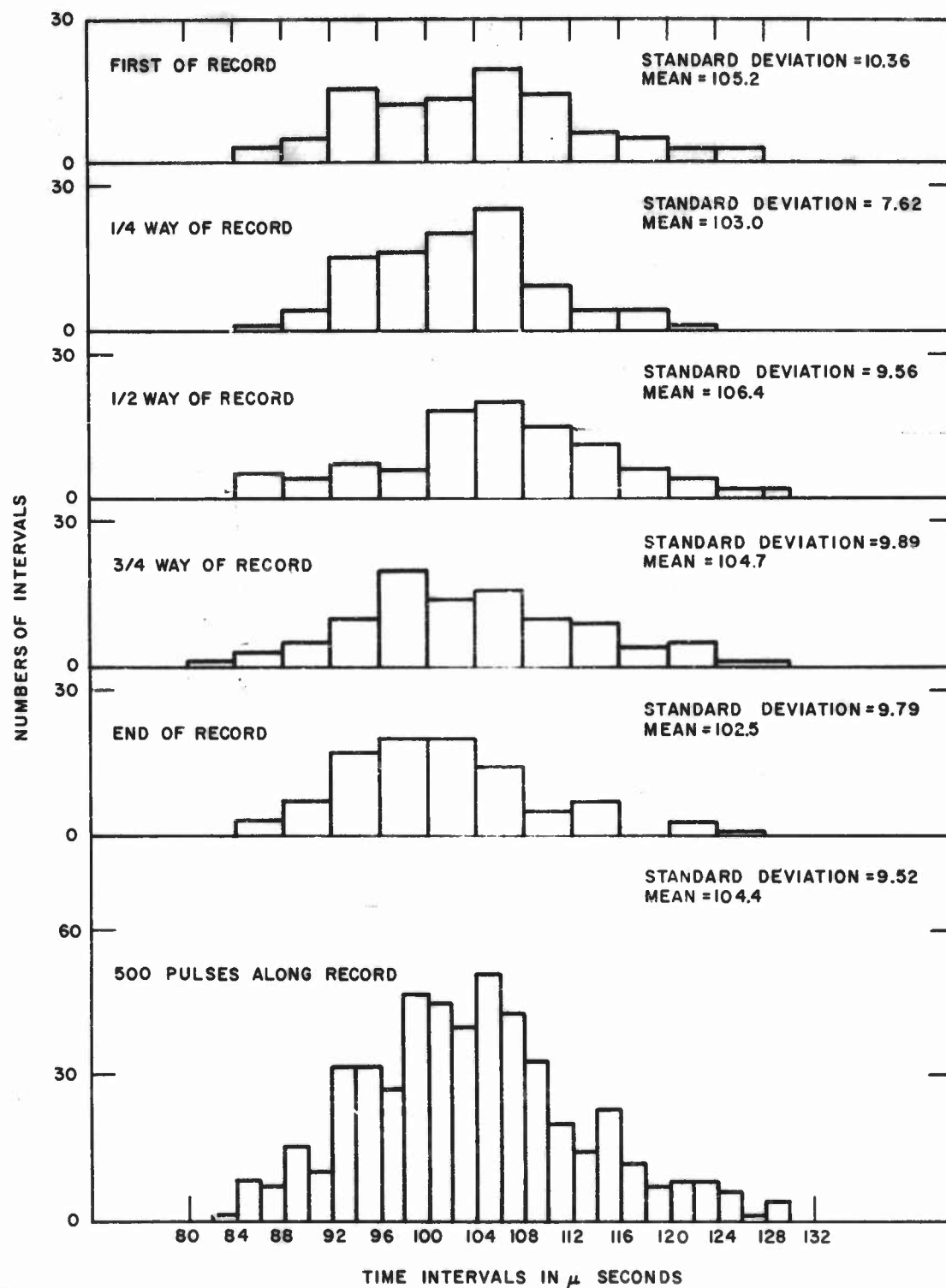


Figure 30 HISTOGRAM OF 10 kc/s UNSYNCHRONIZED PULSE INTERVALS

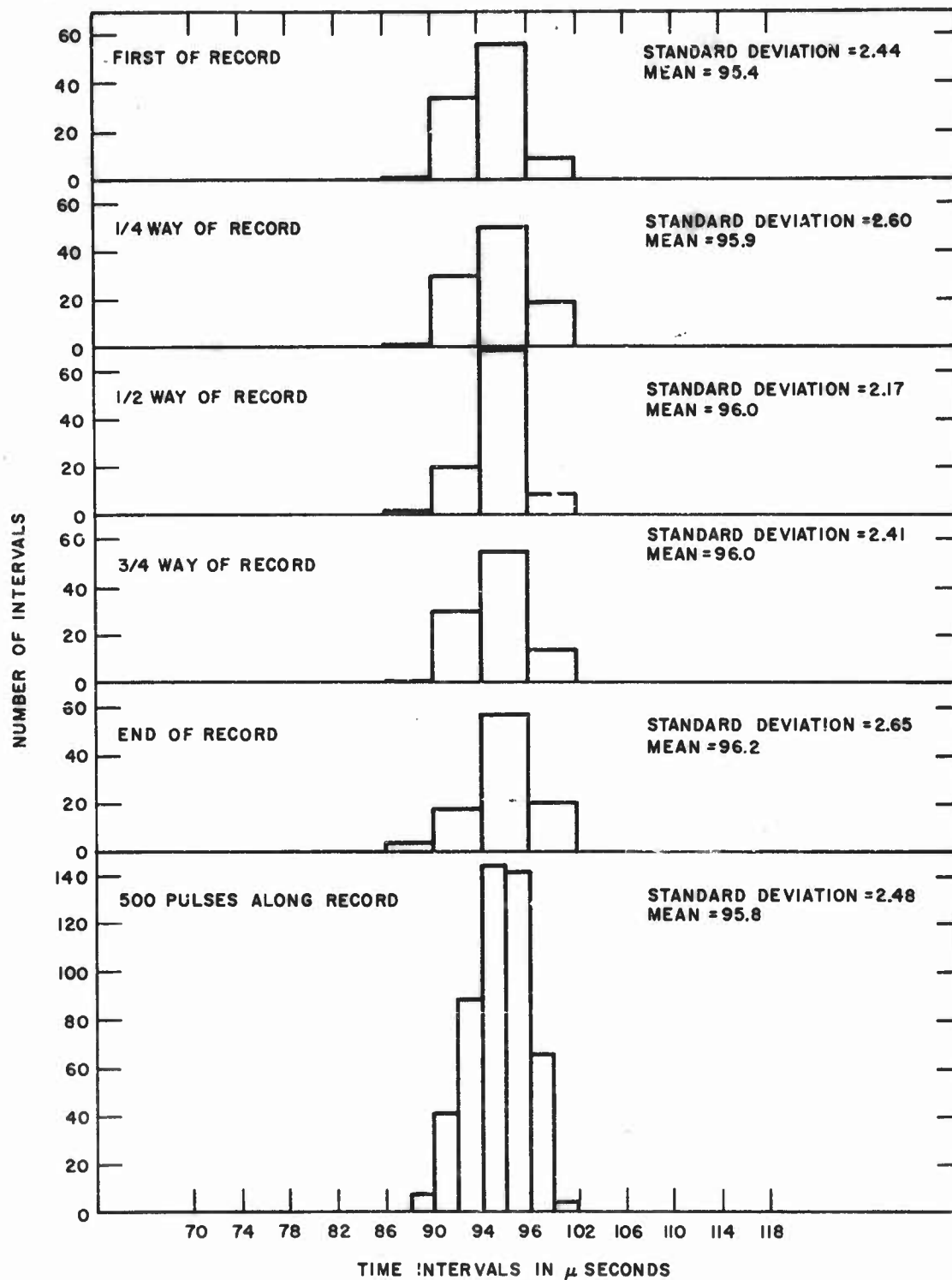


Figure 31 HISTOGRAM OF 10 kc/s SYNCHRONIZED PULSE INTERVALS

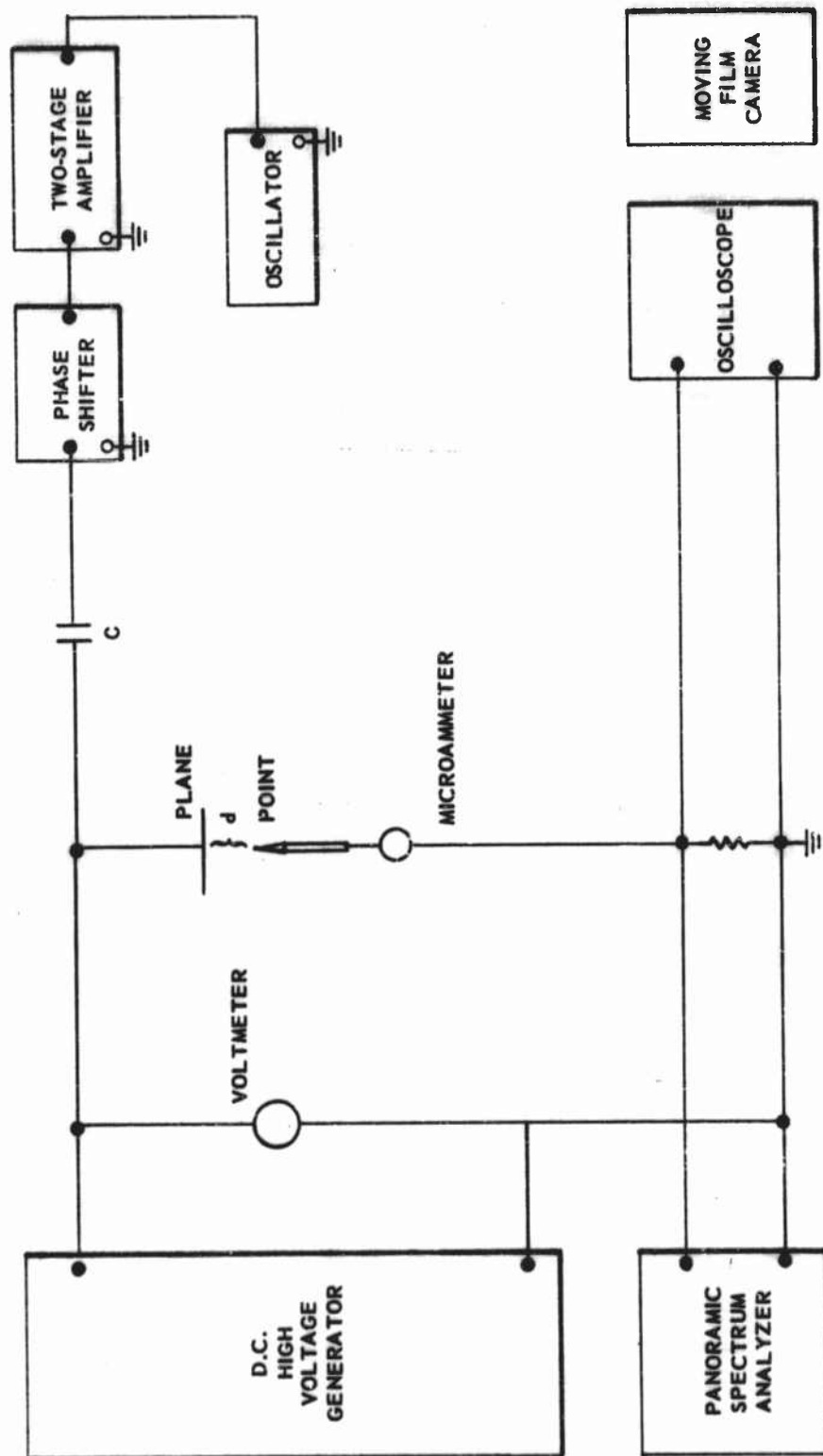
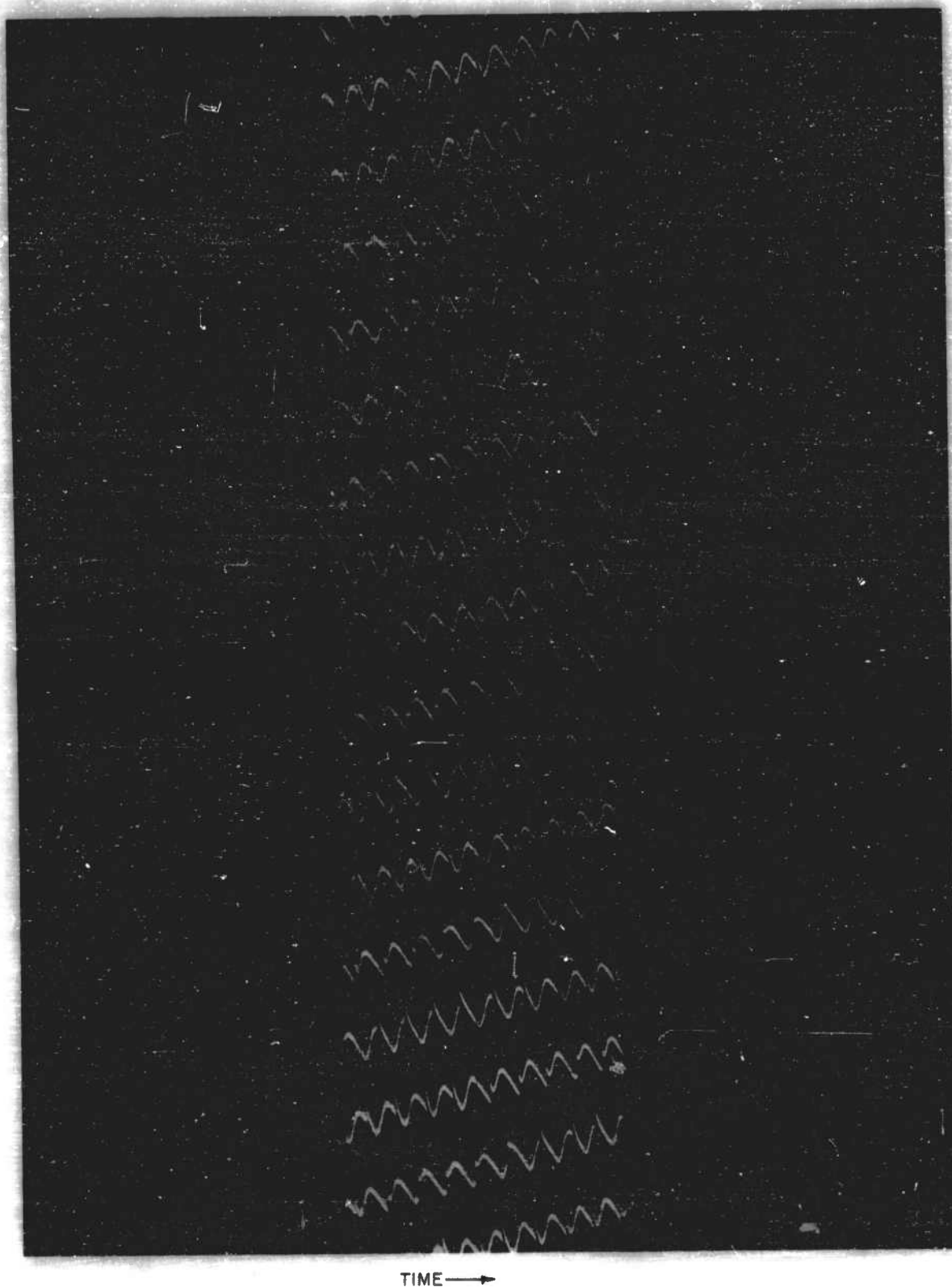


Figure 32 SCHEMATIC DIAGRAM OF EQUIPMENT



TIME →

↑
TIME

Figure 33 UNSYNCHRONIZED TRICHEL PULSES

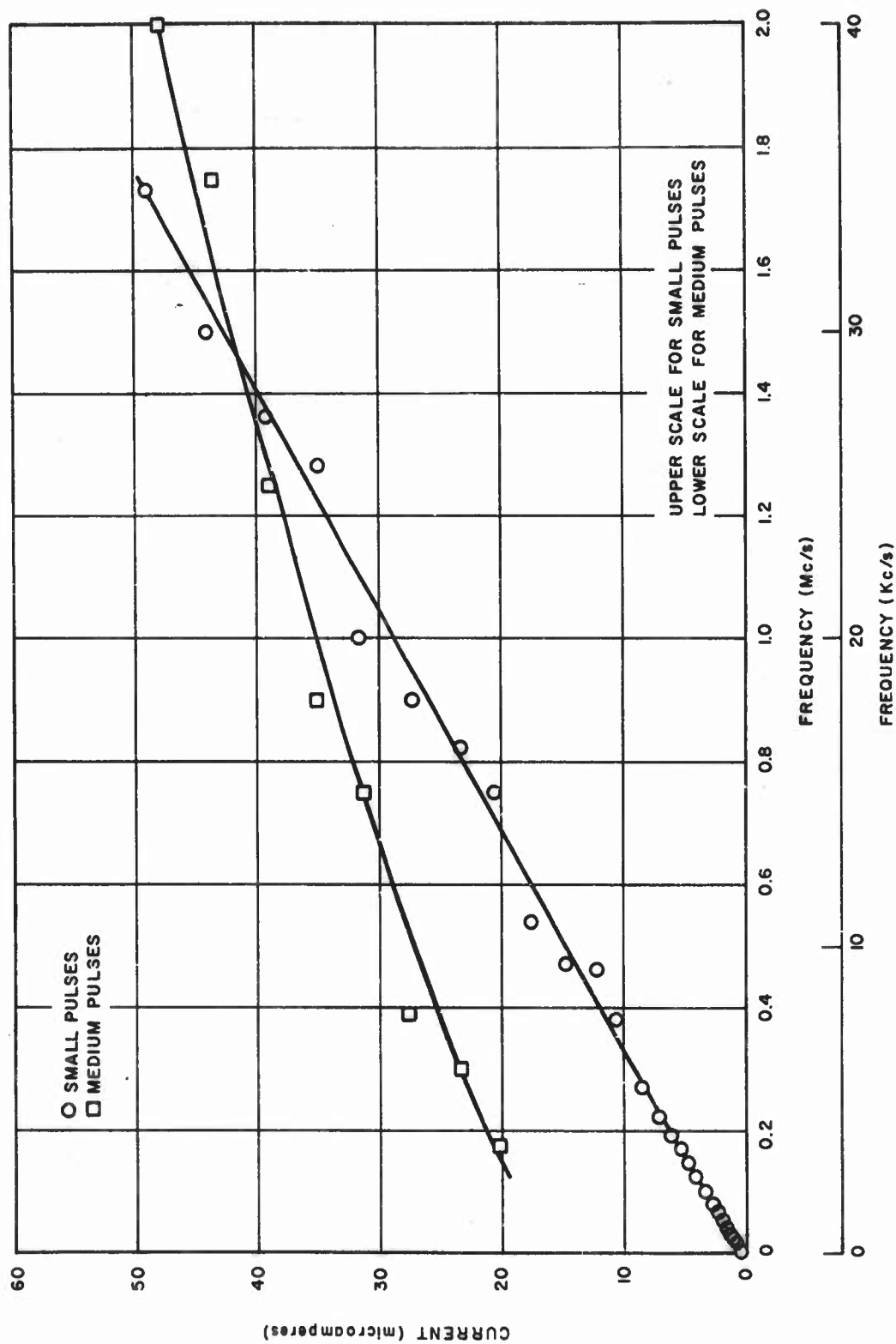


Figure 34 CORONA CURRENT VERSUS TRICHEL PULSE REPETITION FREQUENCY

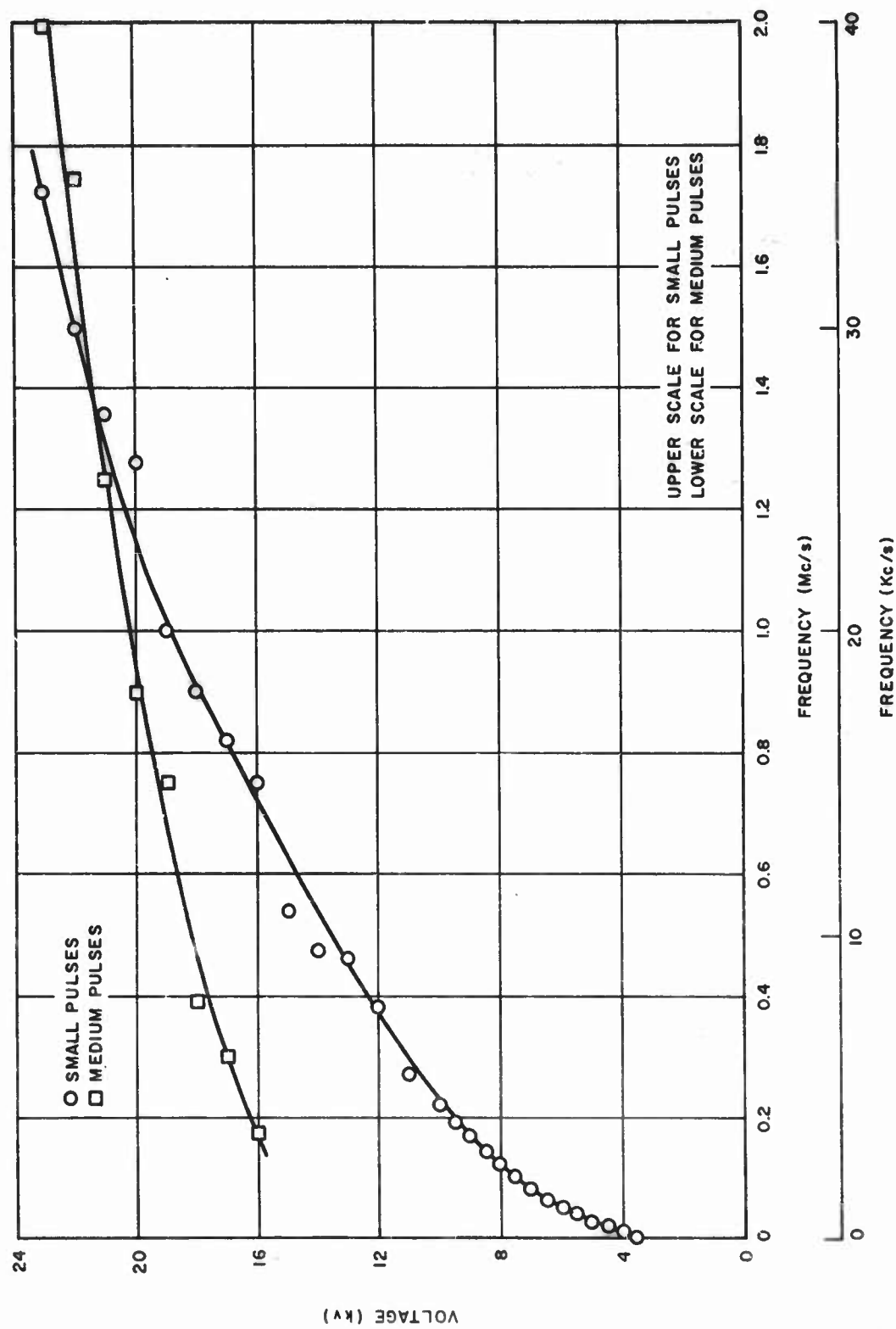


Figure 35 APPLIED VOLTAGE VERSUS TRICHEL PULSE REPETITION FREQUENCY

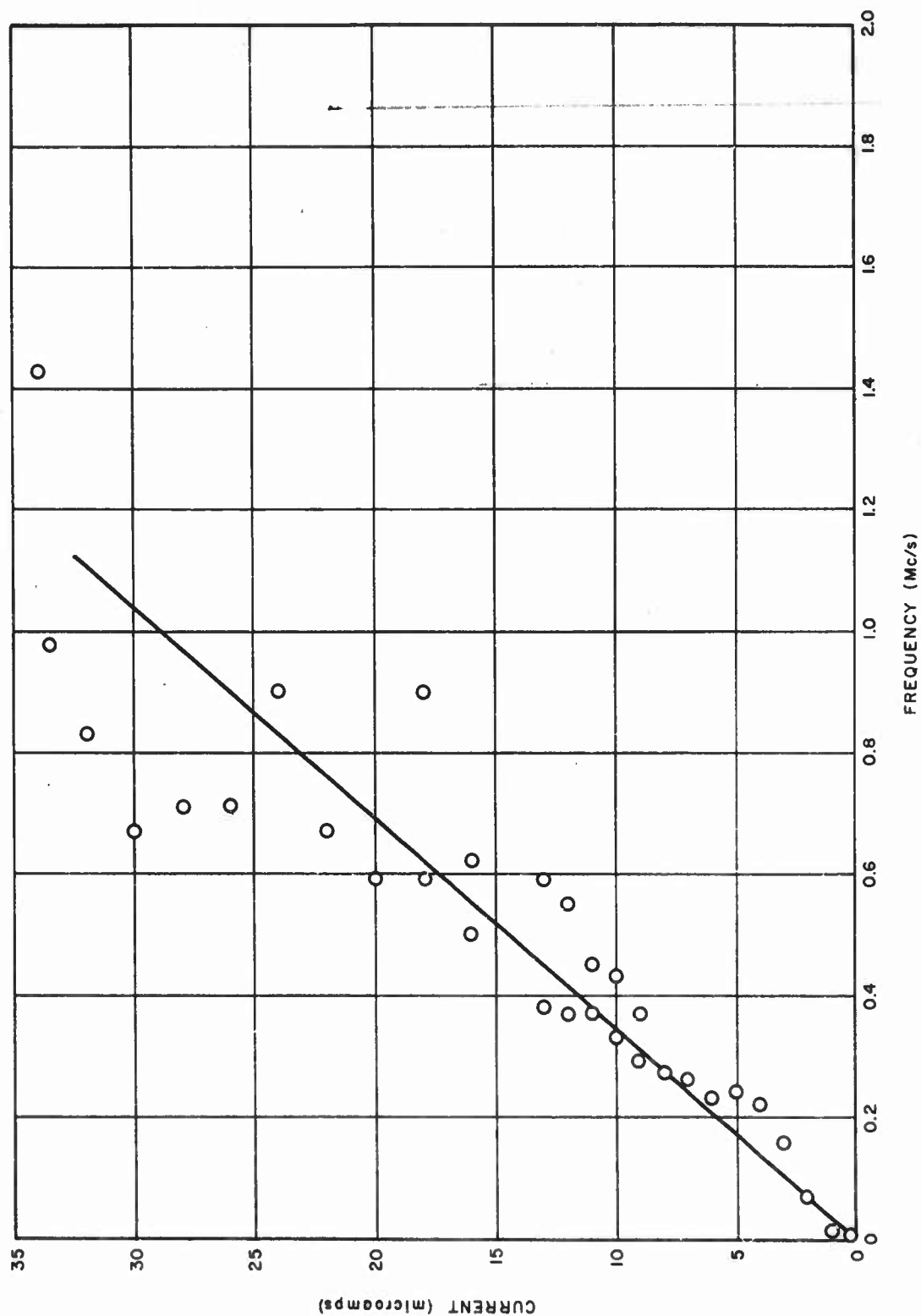


Figure 36 CORONA CURRENT VERSUS TRICHEL PULSE REPETITION
FREQUENCY

3.6 Photoelectric and Audio Technique

There are several other possible ways in which Trichel pulses can be examined in addition to those already employed and discussed above. The eye judging the movement upon a screen of the peak response of a spectrum analyzer, or assessing the repetition rate of a sequence of pulses, is not such a delicate judge of pitch variations as the ear listening to a changing audio frequency. Accordingly, it is potentially advantageous, in order to gain a quick idea of the variations in p-r-f for a given voltage across the gap, to apply the pulses to some kind of audio output such as a loudspeaker.

There are circumstances under which it is convenient to be able to study the Trichel pulse corona without the necessity for any direct electrical connection to the point. This is notably so for the case of the point being at a high voltage and in corona without any adjacent plane. Pick-up with an antenna of the electromagnetic radiation from the pulses has already been described. Another indirect technique is to register the luminosity due to each pulse photoelectrically, and a further possibility is to detect the pressure peaks associated with the "ionic wind" accompanying each pulse.

This section deals with the development of some of these techniques and the kind of results that can be obtained by their use.

Figure 37 is a diagram of the photoelectric technique. The Trichel pulses can be monitored photoelectrically and electrically with a dual input to the oscilloscope. Both inputs are used to determine the reliability of each method in reproducing the Trichel pulses. Photoelectric pulses of 10 kc/sec and 20 kc/sec are shown in figures 38 and 39. There is an indication of two pulse sizes. The vertical lines on the left are timing signals 1/60 sec apart.

Photoelectric and electric pulses of 10 kc/sec and 20 kc/sec are displayed together in figures 40 and 41. The photoelectric pulses are smaller in amplitude than the electric pulses in both photos. In each pair of sweeps, the photoelectric display is on the bottom. Switching between input channels is at the rate of 100 kc/sec so that each channel operates for 5 μ sec at a time. Careful observation shows the photoelectric pulses leading by 5 μ sec. Otherwise the two sets of pulses appear identical.

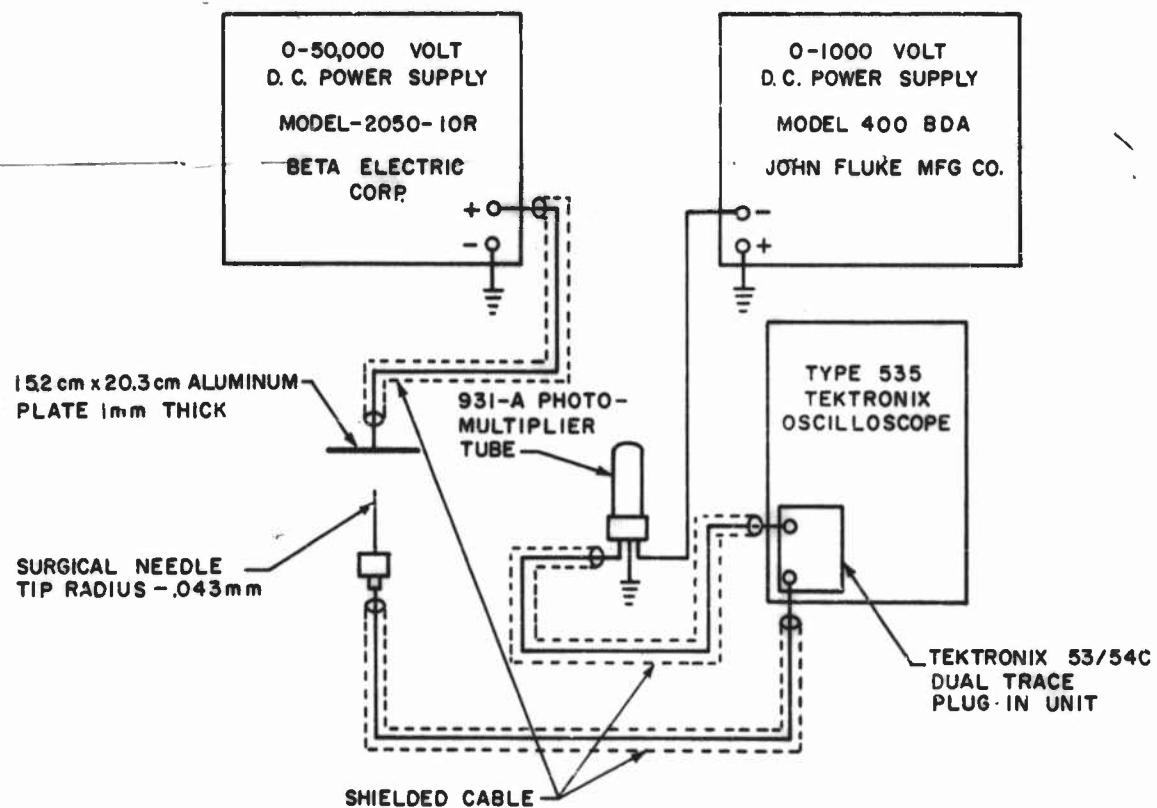


Figure 37 SCHEMATIC DIAGRAM OF PHOTOELECTRIC TECHNIQUE

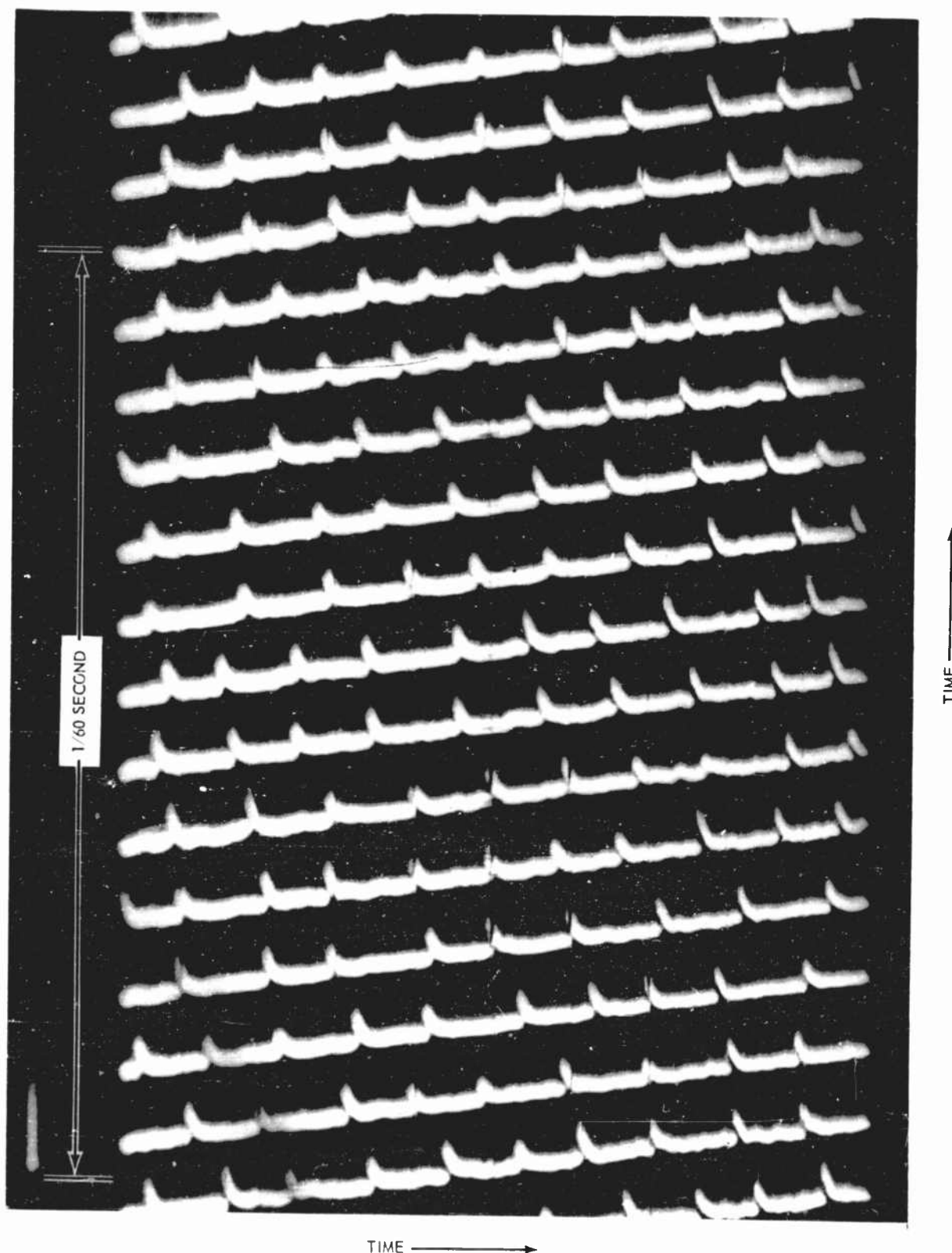


Figure 38 TEN kc/s PHOTOELECTRIC PULSES

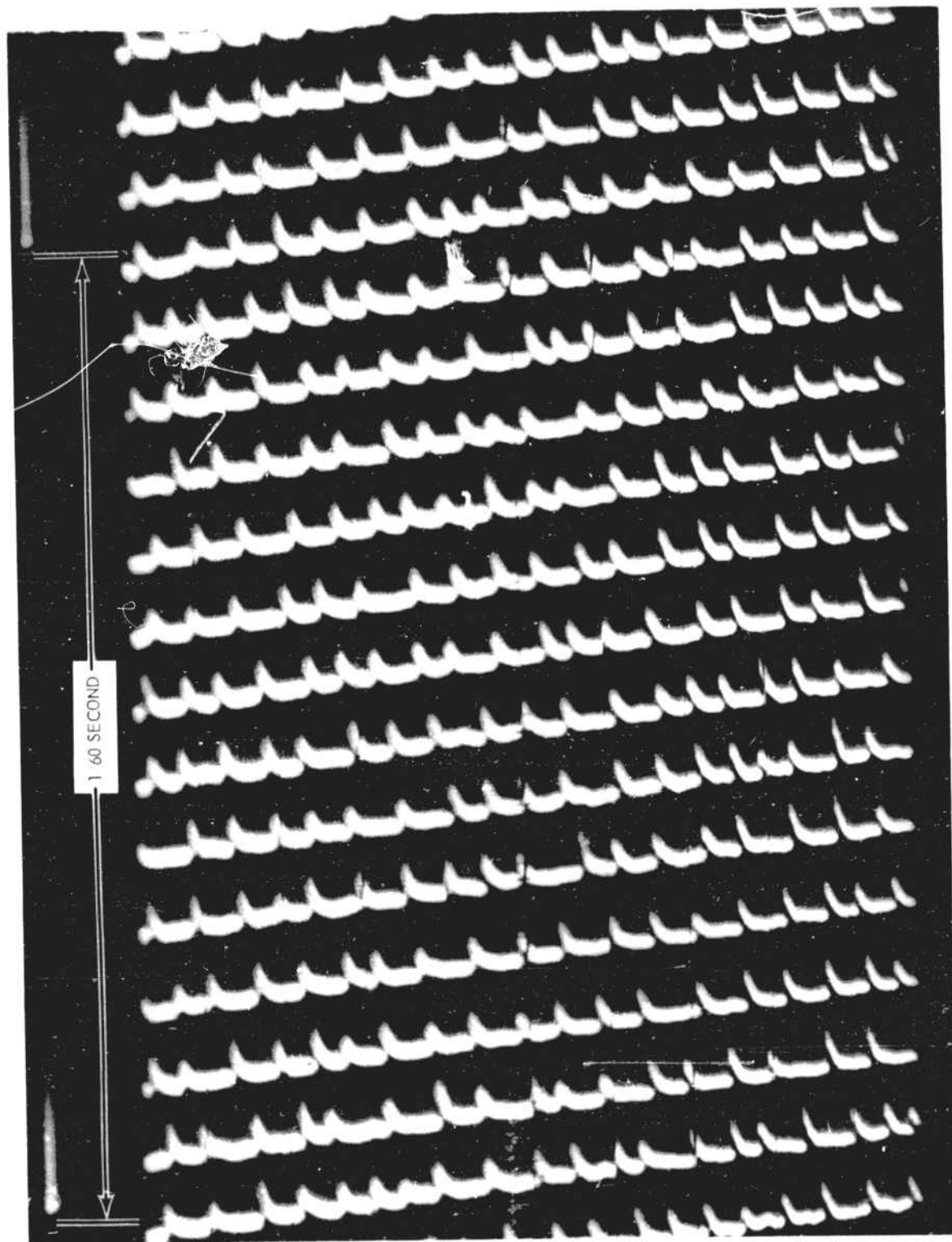


Figure 39 TWENTY kc/s PHOTOELECTRIC PULSES

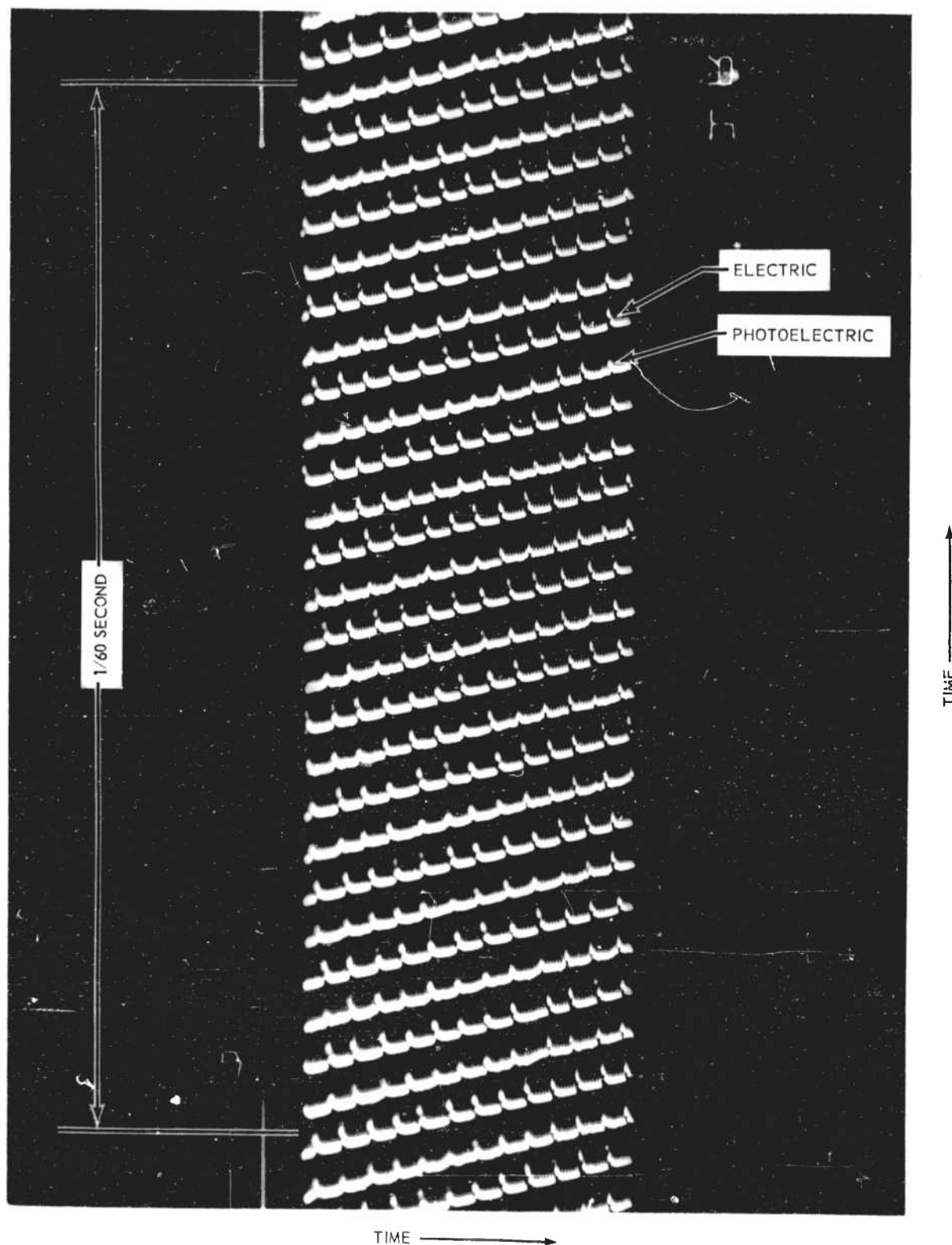


Figure 40 TEN kc/s PHOTOELECTRIC AND ELECTRIC PULSES

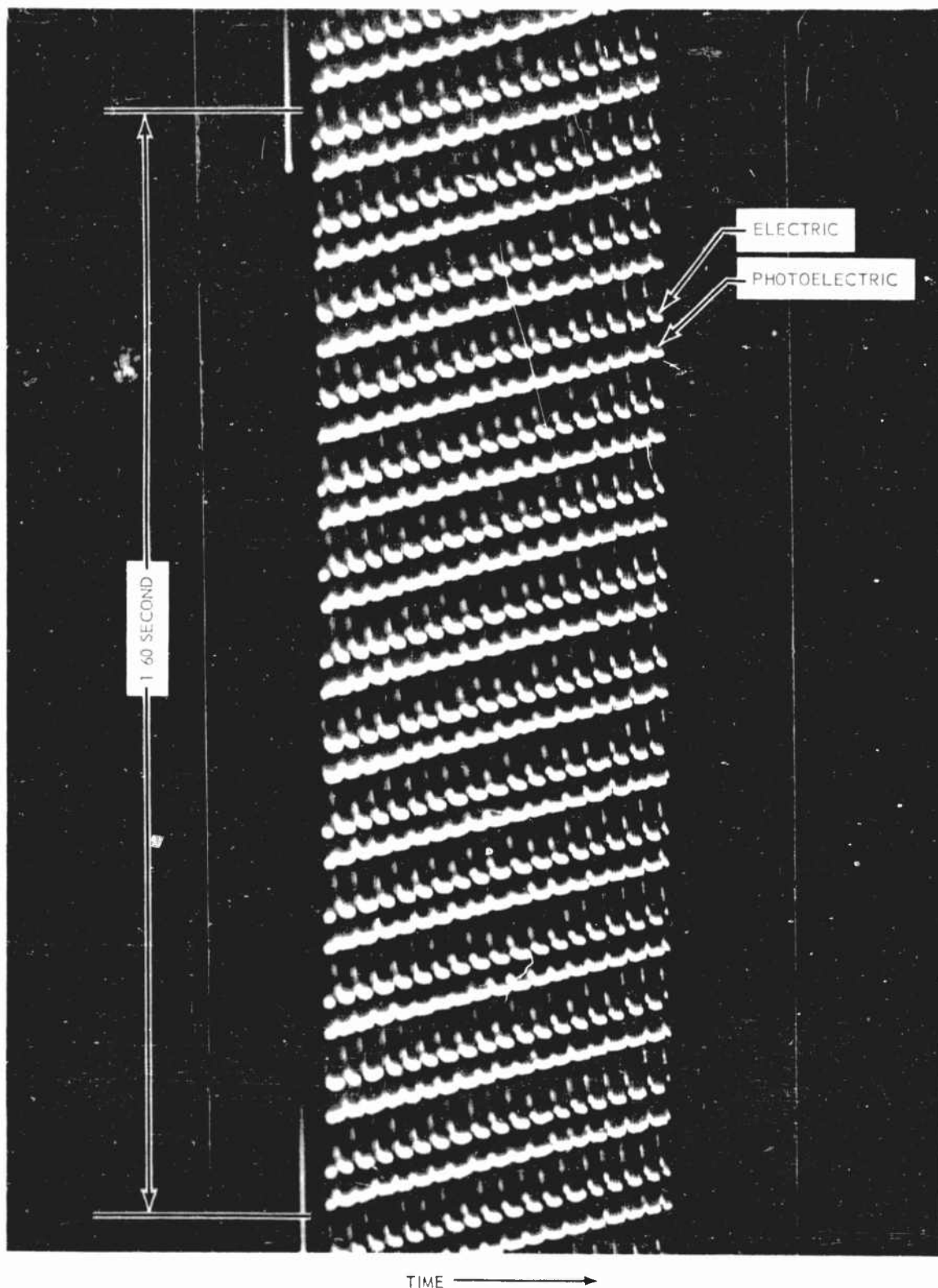


FIGURE 41 TWENTY kc/s PHOTOELECTRIC AND ELECTRIC PULSES

IV. DISCUSSION, CONCLUSIONS, AND SUGGESTIONS FOR FURTHER WORK

In summarizing the research described in the present report these features may be itemized:

1. The standard deviation, Δ , of the Trichel pulse intervals is normally of the order of $\tau/12$ where τ is the mean interval.
2. Application of a sinusoidal stabilizing voltage can reduce Δ to a value of at least $\tau/40$.
3. Multiple families of pulses often appear particularly for rough points at high voltages.
4. Pulse repetition frequencies of a few mc/s were the highest attained in the course of the experiments.
5. Short-lived changes in regime, greatly affecting the nature of the discharge, occur not infrequently.

It must be admitted that the results are not especially favorable as regards the ball lightning hypothesis advanced in Section I. If a frequency of 10 mc/s is taken as the greatest p-r-f possible (this is the maximum observed by Large¹⁶), and a value of $\Delta = \tau/10$ is adopted, then the harmonics beyond 30 or 40 mc/s are hardly distinguishable. In other words, the discreteness of the radio energy has disappeared at a frequency an order of magnitude below that (300 mc/s) required on the Kapitsa mechanism.

Some encouragement is given by the fact that although the average value of Δ may be $\tau/12$, yet, as indicated in Section III, there are short periods within which the natural p-r-f has great intrinsic stability. It is almost certain that the origin of many of the fluctuations commonly observed lies in changes in the condition of the discharging surface and, in this connection, one modern school³⁹ holds that practically all gas discharges are controlled by cathode phenomena. It may well be that examination of the variations in Trichel pulses is a sensitive way of detecting alterations in electrode surface characteristics. The differences in standard deviations for the five selected sections on figures 22 and 25 is some indication of this. Certainly it is true that both fatigue and enhancement of the photoelectric y p mechanism can occur, and the well known effect of "conditioning" of the discharge point⁴⁰ has been identified as a decrease in the work function of the cathode and a consequent increase in y p.²¹

The reproducibility of the results in the experiments could certainly be improved by better experimental arrangements. For instance, the variable surface influences mentioned in the preceding paragraph could be

reduced by using points of a non-oxidizable material such as gold. Again it is felt that space charge contamination was often present in the confined point-plane gap, and was also suspected even for the van de Graaff work; a forced ventilating wind to remove space charges as they are formed would be desirable. For the same reason it would be advantageous to use an isolated high-voltage point, rather than a point-plane gap with the point as the earthy electrode, for the experiments. Photoelectric, radio pick-up, or an acoustic transducer could be used to examine the discharge, and the free access would facilitate examination of any stabilized plasma. Finally, it is perhaps worth mentioning that the points are acted upon by electrostatic forces and that in the zero position, the equilibrium is basically unstable. Any slight displacement will be increased until the returning mechanical force due to bending of the point overcomes the electrostatic forces. Vibrations and oscillations of the point take place.⁴¹ The finer the point the higher the basic p-r-f but the greater the tendency to vibration. This vibration may have very deleterious effects upon attempts to obtain resonant stability by the injection of an artificial signal.

It has already been pointed out that, as regards the application to Kapitza's ball lightning theory, the results do not indicate any continued discreteness at a frequency of the order of 300 mc/s. There are suggestions, however, that the spectrum may have a line character transiently even at as high as 300 mc/s. It is felt that the final test should be the direct examination of the radio-frequency spectrum, omitted by a point in intense corona exposed under natural thunderstorm conditions; the ideal location would be on an isolated mountain-top such as Mt. Withington, New Mexico or Mt. Washburn, Yellowstone Park.

V. REFERENCES

1. Schonland, B. F. J., The Flight of Thunderbolts, Oxford, Clarendon Press (1950).
2. Schonland, B. F. J., The Lightning Discharge, In: Handbuch der Physik, Springer-Verlag, Berlin, XXII (1956).
3. Neugebauer, T., Globular lightning, Z. Physik 106, 474-484 (1937).
4. Nauer, H., Model tests on ball lightning, Z. angew. Physik 5, 441-450 (1953).
5. Hill, E. L., Some Considerations on Ball Lightning, Appendix I, Lightning and Transients Research Institute Report 345 (1957).
6. Hill, E. L., Additional Notes on Ball Lightning, Appendix I, Lightning and Transients Research Institute Report 348 (1958).
7. Gladkov, K., Globe-lightning mystery, Tekhnika-Molodezhi 26, 28-30 (1958).
8. Babat, G., The high-frequency flame, Yung Tekhnik 7, 56-58 (1957).
9. Kapitsa, P. L., On the nature of ball lightning, Dokl. Akad. Nauk SSSR 101, 245-248 (1955).
10. Pierce, E. T., Avco Proposal, (1959).
11. Schonland, B. F. J., and J. Craib, The electric field of South African thunderstorms, Proc. Roy. Soc. (London) 114A, 229-243 (1927).
12. Pierce, E. T., Electrostatic field-charges due to lightning discharges, Quart. J. Roy. Meteorol. Soc. 81, 211-228 (1955).
13. Brook, M. and N. Kitagawa, Lightning and related meteorological conditions J. Geophys. Research 65, 1203-1210 (1960).
14. Large, M. I., and E. T. Pierce, The fine structure of natural point-discharge currents, Quart. J. Roy. Meteorol. Soc. 81, 92-95 (1955).
15. Trichel, G. W., The mechanism of the negative point to plane corona near onset, Phys. Rev. 54, 1078-1084 (1938).
16. Large, M. I., The radio interference produced by corona discharge, J. Atm. Terr. Phys. 10, 245-250 (1957).

17. Kip, A. F., Positive-point-to-plane discharge in air at atmospheric pressure, *Phys. Rev.* 54, 139-146 (1938).
18. Loeb, L. G., A. F. Kip, G. G. Hudson, and W. H. Bennett, Pulses in negative point-to-plane corona, *Phys. Rev.* 60, 714-722 (1941).
19. Loeb, L. B., J. H. Parker, E. E. Dodd, and W. N. English, The choice of suitable gap forms for the study of corona breakdown and the field along the axis of a hemispherically capped cylindrical point-to-plane gap, *Rev. Sci. Instr.* 21, 42-47 (1950).
20. Loeb, L. B., The mechanism of the trichel pulses of short time duration in air, *Phys. Rev.* 86, 256-257 (1952).
21. Amin, M. R., Fast time analysis of intermittent point-to-plane corona in air, III. the negative point trichel pulse corona, *J. Appl. Phys.* 25, 627-633 (1954).
22. Bandel, H. W., Point-to-plane corona in dry air, *Phys. Rev.* 84, 92-99 (1951).
23. Greenwood, A., Pulse-free discharges in negative point-to-plane corona, *Phys. Rev.* 88, 91-92 (1952).
24. Loeb, L. B., Electrical Breakdown of Gases with Steady or Direct Current Impulse Potentials, In: *Handbuch der Physik*, Springer-Verlag Berlin, 22, 445-531 (1956).
25. Large, M. I., The radio interference produced by corona discharge, *J. Atm. Terr. Phys.* 10, 245-250 (1957).
26. Kirkman, J. R., and J. A. Chalmers, Point discharge from an isolated point, *J. Atm. Terr. Phys.* 10, 258-265 (1957).
27. Large, M. I., and E. T. Pierce, The dependence of point-discharge currents on wind as examined by a new experimental approach, *J. Atm. Terr. Phys.* 10, 251-257 (1957).
28. Chapman, S., Cornell Aeronaut. Lab. Rept. No. C.A.L. 68, (1956).
29. Whipple, F. J. W., and F. J. Scrase, Point discharge in the electric field of the earth, *Geophys. Memo, Meteorol. Office (London)*, 68, 1-20 (1936).
30. Wormell, T. W., The Effects of Thunderstorms and Lightning Discharges on the Earth's Electric Field, *Phil. Trans. Roy. Soc. (London)* 238A, 249-303 (1939).

31. Chalmers, J. A., Point discharge currents, J. Atm. Terr. Phys. 2, 301-305 (1952).
32. Cobb, W. E., B. B. Phillips, and P. A. Allee, Mountain-top measurements of atmospheric electricity in northwestern United States, Am. Geophys. Union, Annual Meeting, Washington (May 1959).
33. Moore, C. B., B. Vonnegut, and A. G. Emslie, Observations of thunderstorms in New Mexico, Rept. under Contract NOmr 1684 (1959).
34. Simpson, G. C., and G. D. Robinson, The distribution of electricity in thunderclouds II, Proc. Roy. Soc. (London) 177A, 281-329 (1940).
35. Golde, R. H., Private Communication (1950).
36. Loeb, L. B., Recent developments in analysis of the mechanisms of positive and negative coronas in air, J. Appl. Phys. 19, 882-897 (1948).
37. Cobine, J. D., Gaseous Conductors, Dover, New York (1958).
38. Pierce, E. T., Thunder and Lightning, Shell Aviation News 246, 9 (1958).
39. Jones, F. Ionization and Breakdown in Gases, Wiley, New York (1957).
40. Loeb, L. B., Basic Processes of Gaseous Electronics, Univ. of Calif. Press, Berkeley (1955).
41. Large, M. I., A relaxation oscillation maintained by discharge corona, Nature (London) 179, 707-708 (1957).

DISTRIBUTION

<u>Code</u>	<u>Organization</u>	<u>Copy No.</u>
AF 29	APGC (PGTRI, Tech Lib) Eglin AFB, Fla.	1
AF 69	Director of Resident Training 3380th Technical Training Group Keesler AFB, Mississippi Attn: 0A-3011 Course	2
AF 18	AUL Maxwell AFB, Ala.	3
AF 86	SAC (Operations Analysis Office) Offutt AFB, Nebraska	4
AF 5	AF Missile Test Cen Patrick AFB, Fla. Attn: AFMTC, Tech Library, Mu-135	5
AF 227	USAF Security Service (CLR) San Antonio, Texas	6
AF 28	Hq. USAF (Major R. L. Stell) Tactical Air Group Wash 25, D. C.	7
AF 91	AFOSR (SRY, Mr. Otting) 14th Street and Constitution Avenue Washington, D. C.	8
AF 166	Hq. USAF (AFOAC-S/E) Communications-Electronics Directorate Wash 25, D. C.	9
AF 63	WADD (WCLRSA, Mr. Portune) Wright-Patterson AFB, Ohio	10
AF 43	WADD (WCLJA-2) Attn: Aeronautical Research Lab. Res. Div. Wright-Patterson AFB, Ohio	11
AF 65	WADD (WWDBEG, Mr. N. Draganjac) Wright-Patterson AFB, Ohio	12